Title: Cell type boundaries organize plant development

Authors: Monica Pia Caggiano[1#], Xiulian Yu[1#], Neha Bhatia[1#], André Larsson[2], Hasthi Ram[1], Carolyn Ohno[1], Pia Sappl[1], Elliot M. Meyerowitz[3], Henrik Jönsson[2,4,5], Marcus G. Heisler[1,6 *]

Affiliations:

[1] European Molecular Biology Laboratory, Meyerhofstrasse 1, D-69117 Heidelberg, Germany

[2] Computational Biology and Biological Physics, Department of Astronomy and Theoretical Physics, Lund University, Sweden

[3] Division of Biology and Biological Engineering and Howard Hughes Medical Institute, 156-29, California Institute of Technology, Pasadena, CA 91125, USA.

[4] Sainsbury Laboratory, University of Cambridge, Cambridge, UK

[5] Department of Applied Mathematics and Theoretical Physics, University of Cambridge, UK

[6] School of Life and Environmental Sciences, University of Sydney, NSW, Australia

# - these authors contributed equally to this work

* - author for correspondence: Marcus G Heisler (marcus.heisler@sydney.edu.au)

Once sentence summary: Cell type boundaries regulate plant development

Abstract: In plants the dorsoventral boundary of leaves defines an axis of symmetry through the centre of the organ separating the future top (dorsal) and bottom (ventral) tissues. Although the positioning of this boundary is critical for leaf morphogenesis, the mechanism by which it is established has not been determined. Here we show that dorsoventral boundaries in leaves derive from a boundary between Class III homeodomain-leucine zipper and KANADI expression in the shoot apical meristem, confirming that leaf founder cells are pre-patterned with respect to their dorsoventral axis. Furthermore, perturbation of this boundary not only alters leaf orientation and morphogenesis but also organ position, revealing a general role for these boundaries in plant development. Lastly, we show that auxin stabilizes boundary position at organ

32 inception and that wounds disrupt this process. Overall our findings reveal a two-way
33 interaction between cell type boundaries and auxin that controls fundamental aspects of
34 plant architecture.
35
36
37 **Introduction**
38 Lateral organ development in plants and animals typically involves several processes
39 occurring in a coordinated manner. These include organ positioning, the specification of
40 different cell types and organ morphogenesis. Spatial cues specifying these processes are
41 usually provided by a molecular pre-pattern present in precursor tissues, or from
42 inductive signals emanating from neighboring regions. Unlike animals however, plant
43 organs such as leaves arise continuously in regular patterns around the shoot apical
44 meristem (SAM). These phyllotactic patterns are determined by a self-organizing,
45 iterative process based upon feedback between transcriptional targets of the plant
46 hormone auxin and polar auxin transport (Bhatia et al. 2016). Nevertheless, certain
47 features of leaves are relatively constant including the restriction of their formation to the
48 meristem periphery and their flattened, dorsoventral (top-bottom) orientation with respect
49 to the shoot apex. The spatial cues that specify these features must therefore be provided
50 despite the constant displacement of cells away from the SAM and varying leaf position.
51 Supporting this proposal, wounding experiments involving the isolation of leaf primordia
52 from the meristem have suggested the presence of an inductive signal from the meristem
53 that promotes dorsal identity within leaf primordia at the time of organ initiation
54 (Reinhardt et al., 2005; Sussex, 1951). A variant on this theme is the proposal that auxin
55 depletion in the adaxial (adjacent to the shoot axis) tissues of leaf primordia promotes
56 dorsal identity (Qi et al., 2014). In contrast, other studies suggest that dorsoventral
57 pattering is pre-established, being directly derived from central-peripheral patterning of
58 the shoot (Hagemann and Gleissberg, 1996; Husbands et al., 2009; Kerstetter et al.,
59 2001). Overall, the nature of the initial positional information that specifies leaf
60 dorsoventrality remains unresolved (Kuhlemeier and Timmermans, 2016).
61 Besides influencing leaf differentiation and shape, genes involved in leaf dorsoventrality
62 influence leaf position (Izhaki and Bowman, 2007). For instance, Arabidopsis plants

63 mutant for the KANADI (KAN) genes develop leaves ectopically from the hypocotyl and
64 leaf tissues while plants mutant for the Class III HD-ZIP (HD-ZIPIII) genes develop
65 leaves from the center of the shoot (Izhaki and Bowman, 2007). These observations
66 indicate that the developmental mechanisms that specify leaf dorsoventrality may also be
67 involved in organ positioning although how these processes relate is unclear.
68
69 In this study we investigate the origin of dorsoventral patterning in detail. We find
70 evidence of a developmental pre-pattern of HD-ZIPIII and KAN gene expression in the
71 meristem periphery which, by restricting auxin activity, specifies both the locations of
72 lateral organs as well as their dorsoventrality. We also show that in addition to triggering
73 organ initiation, high auxin levels maintain dorsal cell identity as organs initiate. These
74 results reconcile previous findings and reveal a more general role for HD-ZIPIII / KAN
75 boundaries in determining plant architecture.
76
77 **Results**
78 **Genes involved in leaf dorsoventrality pre-pattern organ formation in the shoot**
79 To better understand the establishment of dorsoventral patterning in developing organs
80 we examined the expression of several genes involved in specifying leaf dorsoventrality
81 in the shoot apical meristem (SAM) using functional fluorescent protein reporters. We
82 found these proteins to be localized in non-overlapping concentric patterns with the
83 dorsal Class III HD-ZIP protein REVOLUTA (REV) (Otsuga et al., 2001) being detected
84 centrally, as marked by the expression of REVp::REV-2×YPet (REV-2×YPet), and the
85 ventral protein KANADI1 (KAN1) (Kerstetter et al., 2001) expressed peripherally, as
86 marked by the expression of KAN1p::KAN1-2×GFP (KAN1-2×GFP) (Figure 1, A to E).
87 Imaging PIN1-CFP together with these reporters revealed regions of high PIN1-CFP
88 expression, marking positions of organ inception (Heisler et al., 2005; Reinhardt et al.,
89 2003), to be centered on a narrow region located between the dorsal and ventral domains
90 (Figure 1D-K). This arrangement was conserved with few cells altering their KAN1
91 expression status during organogenesis (Figure 1C arrowhead and Figure 2 A-F).
92 Ventrally expressed MIR165/166 (Kidner and Martienssen, 2004; Merelo et al., 2016;
93 Nogueira et al., 2007; Yao et al., 2009) also appeared active in the SAM periphery as

94 marked by a *MIR166Ap::GFPER* reporter and MIR165/166 biosensor (Figure 3A-I),
95 consistent with previous studies (Miyashima et al., 2013). Both KAN1-2×GFP and
96 *MIR166Ap::GFPER* re-established their expression in the SAM periphery after organ
97 outgrowth (Figure 1E and Figure 3C). As members of the WOX family of transcription
98 factors are expressed at dorsoventral boundaries (Nakata et al., 2012) we imaged
99 functional translational fusions to both PRS and WOX1 to examine their expression in
100 the shoot relative to leaves. We found that although WOX1-2×GFP expression was
101 limited to the margins and middle domain of leaves (Figure 4A-C), in the vegetative
102 shoot PRS-2×GFP expression extended from the leaf middle domain to surround the
103 SAM in a region between the KAN1 and REV expression domains (Figure 4D-H). In the
104 inflorescence meristem however, PRS-2×GFP expression was restricted to early floral
105 primordia (Figure 4I and J). In contrast to all genes described so far, a FILp::dsRED-N7
106 marker was expressed in both abaxial and adaxial cells at inception, consistent with a
107 previous study (Tameshige et al., 2013) (Figure S1). Overall these data reveal that in
108 many respects although not all, dorsoventral patterning within young leaf primordia,
109 including the middle region, corresponds with central-peripheral patterning in the SAM.

110 **The KAN and Class III HD-ZIP genes repress organ initiation where they are**
111 **expressed**

112 The correlation between organ positioning and KAN-HD-ZIPIII expression boundaries as
113 well as previous genetic data reporting ectopic organs in *kan1 kan2 kan4* and *rev phb phv*
114 mutants (Izhaki and Bowman, 2007) demonstrate a role for these genes in the repression
115 of leaf initiation. However it is possible that the HD-ZIPIII genes influence organ
116 initiation only indirectly by promoting SAM formation during embryogenesis (Emery et
117 al., 2003). To distinguish between these possibilities we induced the expression of
118 MIR165/166-resistant REVr-2×VENUS throughout the epidermis using the ATML1
119 promoter (Sessions et al., 1999) and found that it caused an arrest of organ formation and
120 repression of KAN1-2×GFP in both the vegetative and inflorescence meristems (Figure 5
121 A-E). Similar results were observed after induction of a short tandem target mimicry
122 construct designed to repress MIR165/166 activity (Yan et al., 2012) (Figure 5F and G)
123 or after epidermal induction of MIR165/166-resistant PHAVOLUTA (Figure 5H-J).

124 Similarly, plants expressing KAN1 ectopically in the epidermis also stopped making new
125 organs (Figure 5K and L) and the inflorescence meristem took on a dome shape before
126 eventually arresting (Figure 5M). We conclude both the KAN and Class III HD-ZIP
127 genes regulate organ positioning at least in part by repressing organ initiation where they
128 are expressed.

129 **Expression patterns of REV and KAN1 in the shoot regulate leaf positioning and**
130 **morphogenesis**

131 To test whether boundaries between KAN1 and Class III HD-ZIP expression in the SAM
132 can play an instructive role in positioning new organs and determining their subsequent
133 dorsoventrality, we induced KAN1-2×GFP expression ectopically at the center of the
134 SAM using a pOp6/LhGR two-component (Samalova et al., 2005) system and the CLV3
135 promoter driving LhGR. After KAN1-2×GFP induction, most seedlings initiated several
136 new leaves before their growth stopped. Confocal imaging of seedlings five days after
137 stratification (DAS) on dexamethasone (DEX) induction medium revealed that new
138 organs, marked by high levels of PIN1-CFP expression, formed ectopically at the
139 perimeter of an enlarged and irregular central domain of induced KAN1-2×GFP
140 expression, in which REV-2×YPet expression had been repressed (Figure 6A and B).
141 Although ectopic KAN1-2×GFP was only detected within or bordering organs during
142 their initiation, REV-2×YPet expression was often restricted during later developmental
143 stages (Figure 6C-H) indicating that patterns of KAN1 gene expression within the SAM
144 can influence subsequent organ development. In particular, we noted that the distal
145 margins of developing leaf primordia always correlated with boundaries of REV
146 expression within the epidermis, even when REV expression was abnormally restricted
147 (arrow heads in Figure 6C-H; movie S1). Several classes of phenotype, including leaves
148 with an inverted orientation, could be distinguished at maturity (Figure 6 I-O and
149 Supplementary Figure S2) that correlated with the patterns of REV-2×YPet expression
150 observed during early development. These distinct morphological classes can be
151 explained according to the configuration of the HD-ZIPIII-KAN boundaries at organ
152 inception. Specifically, we infer that the number and orientation of boundaries within

153 organ founder cells (as specified by high auxin levels) determines the configuration of
154 later leaf marginal tissue (Figure 6P-S).

155 **Maximal auxin response is localized to HD-ZIPIII KAN boundaries**

156 The influence of dorsoventral gene expression on organogenesis suggests that the
157 boundaries between their expression domains may function generally to localize auxin
158 response. In support of this proposal it has been reported that in the inflorescence
159 meristem the auxin transcriptional marker DR5 is only responsive to auxin in the shoot
160 periphery (de Reuille et al., 2006). We examined DR5 expression (Liao et al., 2015) in
161 the vegetative meristem by examining its expression both in the wild type and after 1-N-
162 Naphthylphthalamic acid (NPA) treatment at 4 DAS. In mock treated seedlings we found
163 DR5 to be expressed at the locations of incipient primordia and at the distal tip of existing
164 leaf primordia of (Figure 7A and B). In contrast, NPA treated seedlings expressed DR5 in
165 a ring encircling the SAM prior to organ emergence and in the middle domain or
166 dorsoventral boundary region of developing leaves (Figure 7C and D). Similar
167 experiments with seedlings expressing the ratiometric R2D2 intracellular auxin reporter
168 (Liao et al., 2015) revealed a generally broader distribution of auxin compared to the
169 DR5 transcriptional response, especially after NPA treatment, where signal was not
170 restricted to the meristem periphery or leaf tip (Figure 7E-H). Given the similarity in
171 expression between auxin-induced DR5 expression and PRS expression we tested
172 whether PRS as well as WOX1 are auxin inducible and found that both genes respond to
173 auxin treatment within 12 and 15 hrs respectively although their response, like DR5, was
174 mainly restricted to the boundary region (Figure 7I-P). Measuring transcript levels using
175 qPCR indicated that the auxin response for both genes occurs at the transcriptional level
176 (Figure 7Q).

177 **The absence of HD-ZIPIII and KAN expression in boundary regions may mediate**
178 **boundary function**

179 The relatively low level or absence of KAN1 and REV expression observed within
180 boundary regions and the finding that both genes repress organ formation where they are
181 expressed suggests a simple model in which organ formation is localized to boundary

182 regions due to the local absence of KAN and HD-ZIPIII expression in boundary cells. We
183 tested this proposal *in silico* by implementing a previous model for phyllotaxis that
184 incorporates the polarization of PIN1 towards cells with high intracellular auxin
185 concentrations (Bhatia et al., 2016; Jonsson et al., 2006; Smith et al., 2006). By assuming
186 that both KAN1 and REV repress auxin-induced transcription and by including a narrow
187 region of cells located between the KAN1 and REV expression domains the model was
188 able to self-organize the periodic formation of auxin maxima along the boundary as
189 predicted, compared to a broader distribution of maxima when such boundaries are not
190 included (Figure 8A-D; compare 8B to 8D).

191 **Auxin is required to maintain adaxial cell identity during organ initiation**

192 So far, our results indicate that both HD-ZIPIII and KAN1 suppress auxin-induced organ
193 formation in tissues where they are expressed. However this does not exclude the
194 possibility that auxin may play a role in patterning HD-ZIPIII and KAN expression.
195 Indeed, REV expression typically extends towards PIN1 polarity convergence patterns in
196 the meristem periphery and disappears in axil regions where auxin is depleted, suggesting
197 a direct or indirect role for auxin in promoting REV expression (Figure 1) (Heisler et al.,
198 2005). To investigate any potential regulation of REV and KAN expression by auxin we
199 treated inflorescence meristems with a combination of NAA and NPA and found that the
200 region in between the REV and KAN1 domains appeared to narrow due to a slight
201 expansion of REV expression (Figure 9A and B). To test whether REV depends on high
202 auxin levels for its usual pattern of expression we treated triple marker plants with the
203 TIR1 antagonist auxinole (Hayashi et al., 2012) as well as auxin synthesis inhibitors
204 yuccasin (Nishimura et al., 2014) and kyn (He et al., 2011). Although treatment with
205 these drugs individually did not lead to an obvious response, a combination of all three
206 led to a cessation of organ production and an expansion and restriction of KAN1 and
207 REV expression centrally, respectively (Figure 9C and D). KAN expression not only
208 expanded into those cells originally located between the REV and KAN1 domains but
209 also cells that had previously been expressing REV at high levels. However KAN1
210 expression remained excluded from the central most cells of the shoot and established
211 floral primordia, where REV expression still remained (Figure 9D). Extending the drug

212 treatment time did not lead to a further change in expression. A similar response occurred
213 in the vegetative meristem (Supplementary Figure S3). Monitoring the ratiometric auxin
214 sensor R2D2 in response to a similar combined inhibitor treatment indicated a strong
215 decrease in overall intracellular auxin levels, including in the central meristem regions
216 where REV was still expressed (Figure 9E and F). Overall these data indicate that high
217 levels of auxin are necessary to promote REV expression in cells entering the peripheral
218 zone, thereby promoting the establishment of dorsal cell types within initiating primordia.
219 However this influence appears restricted to those cells not already expressing KAN1.

220 **Wounding causes auxin depletion dependent abaxialization**

221 Since wounding causes repolarization of PIN1 away from the wound site (Heisler et al.,
222 2010) resulting in auxin depletion (Landrein et al., 2015) and auxin is required to
223 maintain REV at the expense of KAN expression in peripheral meristem tissues, we
224 investigated whether wounding results in ectopic KAN1 and reductions in REV
225 expression. Firstly, using a pulsed IR laser to ablate cells adjacent to young organ
226 primordia we confirmed that auxin levels decrease in the vicinity of wounds by
227 monitoring the expression of the R2D2 ratiometric marker (Figure 10A and B). Next, we
228 monitored REV, KAN and PIN1 expression in response to such wounds. We found that
229 KAN1 became expressed in cells adjacent to the wound on either side, regardless of
230 wound orientation with respect to the SAM (Figure 10C and D – figure supplement 4A-
231 H). Such a response argues against the possibility that ectopic KAN is the result of
232 interruption of a signal emanating from the meristem that promotes dorsal and represses
233 ventral identity (Sussex, 1955). Instead, it supports the proposal that KAN1 expression is
234 promoted in the vicinity of wounds in general, possibly due to low auxin levels. To test
235 this hypothesis, we repeated these experiments while treating the wounded meristems
236 with combinations of NAA and NPA over a 48 hr period and found that the induction of
237 KAN1 expression around wounds could be completely eliminated if NAA and NPA were
238 combined (Figure 10E and F; figure supplement 4I-M). Although a similar response to
239 wounding was found to occur in vegetative meristems, the wound response typically
240 involved a more substantial reorganization of meristem structure, possibly due to the
241 small size of the vegetative meristem relative to the wounds (figure supplement 5A-C).

242 When new leaves subsequently formed, they were always properly oriented with respect
243 to the new meristem organization.
244
245 **Discussion**
246 In this study we shed new light on a long-standing question regarding leaf dorsoventrality
247 in plants – when and how is it established? The early work of Sussex, based on
248 histological analysis and wounding experiments, suggested that initiating leaf primordia
249 require an inductive signal from meristem tissues to specify dorsal cell fate (Sussex,
250 1955). This proposal has been further supported by a more recent study in tomato
251 (Reinhardt et al., 2005). In contrast, other workers in the field have claimed that
252 dorsoventrality arises directly from radial patterning of the shoot (Hagemann and
253 Gleissberg, 1996). Our results reveal that organs are pre-patterned by domains of KAN
254 and HD-ZIPIII expression in the shoot. The effect of ectopic KAN1 expression at the
255 center of the shoot on subsequent leaf positioning and growth is particularly striking and
256 indicates that the spatial arrangement of HD-ZIPIII and KAN expression present within
257 organ founder cells is incorporated into organs as they initiate and directs patterns of
258 morphogenesis. The propagation of this pattern into initiating organs requires high auxin
259 levels at early stages of development. If auxin levels decrease during organ
260 establishment, REV expression also decreases and KAN1 expression extends towards the
261 meristem center. Thus, the same signal that triggers organ initiation is also required for
262 proper organ differentiation. Nevertheless, at a later stage of development REV
263 expression in both leaf and floral primordia becomes auxin independent. Overall all our
264 results imply that leaf dorsoventrality results from a four-step process: (i) signals during
265 embryonic development establish concentric patterns of Class III HD-ZIP and KAN gene
266 expression (Zhang et al., 2017); (ii) the boundary between these domains helps to define
267 sites for auxin-dependent organogenesis i.e. the meristem peripheral zone; (iii) high
268 levels of auxin at organ initiation sites enables the maintenance of Class III HD-ZIP
269 expression in adaxial (located towards the central shoot axis) primordial cells as these
270 cells are displaced from the central zone; (iv) patterns of HD-ZIPIII and KAN gene
271 expression in developing flowers and leaves are stabilized and dictate future patterns of
272 organ morphogenesis.

273 How do DV boundaries control organ position and shape? Both our data as well as
274 previous studies indicate this is through the regulation of auxin perception. For instance,
275 organ initiation requires high auxin levels but auxin can only trigger organogenesis in the
276 peripheral zone (Reinhardt et al., 2000) where the HD-ZIPIII/KAN boundary occurs. A
277 similar relationship holds for leaves where auxin application results in growth but only
278 from the leaf margins, again corresponding to a DV boundary (Koenig et al., 2009). We
279 further show that the localization of auxin response to DV boundaries applies generally,
280 i.e. DR5 expression appears higher at such boundaries compared to the broader predicted
281 auxin distribution, as marked by R2D2. How is this restriction achieved? Imaging data
282 reveals that the locations of PIN1 polarity convergences correspond to a region of cells in
283 which the expression of both HD-ZIPIII and KAN is low or absent. Given genetic and
284 molecular data indicating that both the HD-ZIPIII and KAN genes repress auxin activity
285 (Huang et al., 2014; Merelo et al., 2013; Zhang et al., 2017), we propose that the absence
286 of their expression in boundaries results in a local de-repression of auxin-induced
287 transcription. In turn, this de-repression would be expected to potentiate feedback
288 between auxin signalling and cell polarity including microtubule orientations that would
289 result in localized outgrowth at the boundary (Bhatia et al., 2016). Such growth may
290 either occur in the periodic fashion typical of phyllotaxis and complex leaves, or in a
291 more continuous manner typical of simple leaves, depending on the strength of auxin
292 transport or other modifications to the feedback system (Bilsborough et al., 2011; Koenig
293 et al., 2009).

294 The conclusions stated above contrast with those of another study reporting that high
295 levels of auxin inhibit dorsal fate and promote ventral cell fate (Qi et al., 2014). These
296 findings were based on auxin application experiments in tomato that resulted in the
297 ventralization of leaves as well as the observation that Arabidopsis *pin1* and *pid rev*
298 double mutants produce trumpet or rod-shaped shaped leaves. Although our results
299 cannot easily explain the tomato data, since high auxin levels are required to maintain
300 REV expression during organ establishment, we would expect that in *pin* and *pid*
301 mutants, lower auxin levels may well result in lower expression levels of REV and
302 possibly other Class III HD-ZIPs, leading to leaf ventralization as reported in these

303 mutant backgrounds (Qi et al., 2014). Further auxin application experiments in tomato
304 that include an analysis of gene expression and auxin level changes may clarify the
305 relationship between auxin and dorsoventral patterning in tomato compared to
306 Arabidopsis.

307 The regulation of HD-ZIPIII and KAN expression by auxin is not only relevant to
308 understanding wild type organ development but also for understanding the reorganization
309 of tissue types in response to wounds. Wounds in the meristem outer cell layer
310 specifically alter cell polarities such that PIN1 becomes polarized away from wounds in
311 adjacent cells (Heisler et al., 2010), leading to auxin depletion (Landrein et al., 2015).
312 Since the 1950s wounding has also been associated with changes in leaf dorsoventrality
313 (Sussex, 1955) and changes to organ position (Snow, 1931). Specifically, wounds located
314 between the meristem and initiating organ were found to promote leaf ventralization and
315 a loss of lamina shape suggesting that the establishment of dorsal cell fate requires an
316 inductive signal from the meristem, which the wound interrupted (Sussex, 1955). Our
317 observations now indicate rather, that during organ establishment, HD-ZIPIII expression
318 depends on high levels of auxin, which wounding disrupts. Thus as suggested previously,
319 the meristem "acts by maintaining in the leaf-forming zone some polarized micro-
320 structure which collapses without it" (Snow and Snow, 1959).

321

322 **Materials and Methods**

323 **Plant material**

324 Plants were grown on soil at 22 °C in continuous light-conditions and cultivated either on
325 soil or on GM medium (1 % sucrose, 1× Murashige and Skoog basal salt mixture, 0.05%
326 MES 2-(MN-morpholino)-ethane sulfonic acid, 0.8 % Bacto Agar, 1 % MS vitamins, pH
327 5.7 with 1 M potassium hydroxide solution).

328 **Construction of Transgenes**

329 Multiply transgenic lines were generated by Agrobacterium-mediated transformation into
330 stable transgenic lines or by genetic crossing. The *FILp::dsREDN7* and *PIN1p::PIN1-*
331 *GFP* transgenes have been described elsewhere (*16*). *pREV::REV-2×VENUS* in the T-
332 DNA vector *pMLBART* (Gleave, 1992) is a modification of *pREV::REV-VENUS* (Heisler
333 et al., 2005) that contains a translational fusion to 2 tandem copies of the fluorescent
334 protein VENUS (Nagai et al., 2002). *REVp::REV-2×Ypet* containing a C-terminal fusion
335 to the 2× Ypet (Nguyen and Daugherty, 2005) in *pMOA36* T-DNA (Barrell and Conner,
336 2006) was transformed into a *PINp::PIN1-CFP* line (Gordon et al., 2007). The
337 *KAN1p::KAN1-2×GFP* transgene in pMOA34 T-DNA was created by amplifying 8.7 kb
338 of *KAN1* (At5g16560) genomic sequences with primers KAN1g F and KAN1g R
339 (Supplementary Table S1) as a translational fusion to a 9 Ala linker and 2×GFP followed
340 by *OCS* terminator sequences. When transformed into *kan1-2 kan2-1* segregating plants,
341 this construct complements the mutant phenotype. The triple marker line was generated
342 by transforming *KAN1p::KAN1-2×GFP* into a *REVp::REV-2×Ypet; PIN1p::PIN1-CFP*
343 transgenic line. *KAN1p::KAN1-2×CFP* or *KAN1p::KAN1-2×Ypet* containing a fusion to
344 2 copies of CFP or Ypet, respectively, were constructed similarly. *KAN1p::KAN1-*
345 *2×Ypet* and *PIN1p::PIN1-GFP* were combined in T-DNA vector *BGW* (Karimi et al.,
346 2002) by Gateway technology (Invitrogen) for generation of a double marker transgenic
347 line.
348 The *KAN1* cDNA was amplified by PCR with primers K1 cDNA F and K1 cDNA R to
349 generate C-terminal translational fusion to a 9 Ala linker followed by single GFP or
350 2×GFP followed by pea *rbcS E9* terminator sequence (Zuo et al., 2001) and cloned into
351 the pOp6/LhGR two-component system (Craft et al., 2005) for dexamethasone-inducible
352 misexpression.
353 An *ATML1p::LhGR* driver containing 3.4 kb of the L1-specific *ATML1* gene
354 (At4g21750) fused to the chimeric LhGR transcription factor and a *6Op::KAN1-GFP*
355 expression construct in a *pSULT* sulfadiazine-resistant T-DNA vector (*ATML1>>KAN1-*
356 *GFP*) was generated. The *pSULT* T-DNA vector was derived from *pMLBART* by
357 replacing the *NOSp::BAR* gene with *1'-2'p::*SUL (Rosso et al., 2003), a plant selectable
358 marker that confers resistance to sulfadiazine herbicide to create *pSULT*. *A*
359 *CLV3p::LhGR* driver containing 1.49 kb of upstream regulatory sequences was PCR

360 amplified with primers CLV3p F and CLV3p R along with 1.35 kb of downstream
361 regulatory sequences with primers CLV3utr F and CLV3utr R was combined with
362 *6Op::KAN1-2×GFP* in *pSULT* T-DNA vector (*CLV3>>KAN1-2×GFP*).
363 *ATML1>>REVr-2×VENUS* is a sulfadiazine-resistant T-DNA vector to misexpress
364 microRNA resistant REV-2×VENUS fusion, where *6Op::REVr-2×VENUS* was
365 constructed by cloning a 1148 bp *Bam*HI-*Xcm*I microRNA resistant REV cDNA (a gift
366 from J. Bowman) harbouring two previously characterized silent mutations that disrupt
367 the binding of MIRNA 165/166 to the coding sequence of *REV* as previously described
368 (Emery et al., 2003) downstream of the *6Op* and in frame with the wild type *REV-*
369 *2×VENUS* coding sequences.
370 *miR166Ap::GFPER* T-DNA construct was kindly provided by K. Nakajima (Miyashima
371 et al., 2011). The MIR165/166 biosensor was created based on the design presented by
372 Smith Z. R. et al. (Smith and Long, 2010) in the AlcR/AlcA expression system (Roslan et
373 al., 2001) for ethanol-inducible expression. The sequences conferring MIR165/166
374 sensitivity from the *REV* coding sequence (*REV*) and the sequences conferring
375 MIR165/166 insensitivity (REVr) were fused to *mCherry* (Shaner et al., 2004) with
376 endoplasmic reticulum localization sequences *mCherryER*, which was synthesized de
377 novo (Genscript). The MIR165/166-*mCherryER* biosensors (both biosensor and control)
378 were cloned as *Hind*III-*Bam*HI fragments downstream of the *AlcA* regulatory sequences
379 in the *UBQ10p:AlcR_BJ36* plasmid vector. *UBQ10p:AlcR* was constructed by cloning the
380 *UBQ10* promoter 2 kb fragment upstream of *AlcR* and the *OCS* terminator. Both
381 *UBQ10p::AlcR* and *AlcA::REV-mCherryER* or *AlcA::REVr-mCherryER* components
382 were combined in the T-DNA vector *pMOA34*.
383 The *WOX1p::2×GFP-WOX1* construct in *pMLBART* T-DNA vector was generated as
384 follows: 2.2 kb of *WOX1 (At3g18010)* upstream promoter sequence was amplified with
385 primers WOX1p F and WOX1p R and cloned using restriction enzymes KpnI and
386 BamHI. 3.6 kb of *WOX1* coding sequence plus 1.65 kb 3'-regulatory sequences was
387 amplified from wild-type Col-O genomic DNA with the primers WOX1g F and WOX1g
388 R and cloned using restriction enzymes *Bgl*II and *Spe*I. 2 copies of GFP were inserted in
389 frame at the start of the *WOX1* coding sequence at the *Bam*HI and *Bgl*II sites. A double

390 marker was generated by transforming the *WOX1p::2×GFP-WOX1* into *a PIN1p::PIN1-*
391 *C*FP transgenic line.
392 The *PRSp::PRS-2×GFP* construct in *pMOA34* T-DNA vector was made by amplification
393 of 3.9 kb *PRS (At2g28610)* genomic sequence (similar to (Shimizu et al., 2009)) with
394 primers PRSg F and PRSg R to create a C-terminal fusion to *2×GFP* followed by *OCS*
395 3'regulatory sequences. Marker combinations were generated by transforming the
396 *PRSp::PRS-2×GFP* into either a *PIN1p::PIN1-CFP* transgenic line or into *REVp::REV-*
397 *2×YPET PIN1p::PIN1-CFP* line. *(PRSp::PRS-2×GFP)* and *(KAN1p::KAN1-2×CFP)*
398 were combined in T-DNA vector BGW (Karimi et al., 2002) by Gateway technology
399 (Invitrogen) for generation of a double marker transgenic lines.
400 A short tandem target mimic (STTM) construct to target MIR165/166 (Yan et al., 2012)
401 was generated in the *pOp6/LhGR* two-component system for dexamethasone-inducible
402 expression with a *UBQ10p::GRLh* driver. *STTM MIR165/166-88* sequence (Yan et al.,
403 2012) was synthesized de novo (Genscript) and cloned downstream of *6×Op* to create
404 *6×Op::STTM 165/166*. Both components were combined in a sulfadiazine T-DNA
405 *pSULT* (*UBQ10>>STTM 165/166*).
406 *ATML1>>PHVr* is a sulfadiazine-resistant T-DNA vector containing a mutated version
407 of *PHV* cDNA (a gift from J. Bowman) with a Gly to Asp amino acid change that
408 disrupts the miRNA165/166 binding site in the *PHV* gene (McConnell et al., 2001).
409 *6×Op::PHVr* was constructed by cloning a 2.6 kb *Xho*I-*Bam*HI *PHVr* cDNA downstream
410 of *6×Op* and upstream of *pea3A* terminator sequences. *ATML1>>PHVr* was transformed
411 into a *REVp::REV-2×YPet; PIN1p::PIN1-CFP* transgenic line.

412 *DR5-3×VENUS v2* reporter gene (Liao et al., 2015) was a generous gift from D. Weijers.
413 The line *R2D2 PIN1p::PIN1-GFP* was described previously (Bhatia et al., 2016).

414 **Dexamethasone induction**
415 For inducible gene perturbations in the vegetative SAM, seeds were germinated directly
416 on GM medium containing 10 µM Dexamethasone (Sigma, stock solution was prepared
417 in Ethanol).. Seedlings were then dissected for imaging at 4 DAS, 5 DAS or 7 DAS
418 depending on the experiment. For DEX induction in the IM, 10 µM DEX solution
419 containing 0.015% Silwet L-77 was applied to the IM every second day three times.

420 Inflorescences were then dissected and imaged. The number of T2 inducible transgenic
421 lines that exhibit the presented phenotypes and the frequencies of phenotypes amongst
422 imaged plants is shown in Table S2 and associated caption.

423 **Confocal Microscopy**

424 Plants were dissected for imaging as previously described (Bhatia et al., 2016; Heisler
425 and Ohno, 2014) and imaged with a Leica SP5 Upright confocal microscope using an
426 Argon laser. The objective used was a water-immersion HCX IRAPO L25x/0.95 W
427 (Leica). Excitation for CFP is 458 nm, GFP is 488 nm, YFP (Ypet and VENUS) is 514
428 nm and tdTomato is 561 nm. Emission signal were collected at 460-480 nm for CFP,
429 490-512nm for GFP, 516-550 nm for YFP (YPet and VENUS), and 570-620 nm for
430 tdTomato. The resulting z-stacks were processed using the Dye Separation (Channel
431 mode or automatic mode) function available in the LAS AF program in order to separate
432 the GFP channel from the YFP (Ypet or VENUS) channel. Three software packages:
433 LAS AF from Leica, Imaris 8.0.2 by Bitplane and FIJI (https://fiji.sc) were used for data
434 analysis. Ratios for R2D2 were calculated as described previously (Bhatia et al., 2016).

435 **Measurement of distance between organs**

436 For distance measurements between oppositely positioned leaves on plants transgenic for
437 inducible KAN1 (*CLV3>>KAN1-2×GFP* – see above) the measurement tool from Imaris
438 8.0.2 (Bitplane) was used. For comparisons to control, untreated seedlings grown on GM
439 were compared to seedlings grown on DEX for 5 days. t-Test was performed using Excel.

440 **Chemical treatments for auxin depletion in the inflorescence meristems**

441 500mM stock solutions of auxinole, yucasin and L-Kynurenine were prepared separately
442 in DMSO. The stocks were diluted in 1mL 0.1M phosphate buffer in sterile water to
443 make a working solution containing all the three drugs (0.2μL of each stock) to a final
444 concentration of 100mM each. The final concentration of DMSO in the working solution
445 containing all the three drugs was 0.06%.

446 Treatments were carried out on the inflorescence meristems of whole plants transplanted
447 from soil to boxes containing GM medium supplemented with vitamins. The older

448 flowers were removed as described (Heisler and Ohno, 2014). The plants were chosen
449 such that the stem of the meristem was a few millimeters above the rosette to prevent the
450 drug solution from dispersing into the surrounding medium. After imaging, the meristems
451 were carefully dried using a thin strip of sterile filter paper to remove excess water.
452 Approximately 50µL of the drug solution was added directly to the meristem, drop-wise.
453 The meristems were treated only once in a time course of 12-18 hours.

454 **NPA treatment on seedlings carrying R2D2 and DR5 markers**

455 Seedling aged 3.5-4DAS were dissected to expose the meristem and the first leaf pair as
456 described (Bhatia et al., 2016). After imaging, seedlings were transferred to new GM
457 medium containing plates and blotted dry with thin strips of sterile paper. 5-10µL of 100
458 µM NPA in sterile water (100 mM stock in DMSO) was added directly to the dissected
459 seedlings every twenty-four hours for three days in total.

460 **Auxin treatment on seedlings carrying PRS and WOX1 markers**

461 Seedlings aged 4DAS (days after stratification) were dissected to expose the meristem
462 and the first leaf pair as described (Bhatia et al., 2016). 5mM NAA solution was prepared
463 in liquid GM medium. Seedlings were then immersed in 100µL of NAA containing
464 medium in individual wells in 96 well plate and grown under continuous light without
465 shaking for 12 hours.

466 **Pulsed Laser ablations.**

467 Laser ablations on the inflorescence meristems were carried out using the Mai Tai multi-
468 photon laser from Spectra Physics, which was controlled with LEICA SP5 confocal
469 software. Z-stacks were acquired prior to ablation. Single cells were targeted one after
470 the other using bleach point mode. Ablations were carried out at 800nm with an output
471 power of ~3W. Each pulse was shot for 1-15 milliseconds. Usually ablations were
472 accomplished within 1-3 bursts of the laser. Ablated cells could be visually identified as
473 their nuclei exploded resulting in unusual auto fluorescence. Z stacks were acquired
474 immediately after the ablations.

475 **Auxin and auxin plus NPA combined treatments on ablated inflorescence meristems**
476 After ablations, the meristems were carefully blotted dry using thin strips of sterile filter
477 paper. 20µL 5mM NAA in sterile water (0.5M stock in 1M KOH) or 20µL of a solution
478 containing 5mM NAA and 100µM NPA in sterile water (100mM NPA stock in DMSO)
479 or mock solution were added directly to the meristems every 24 hours for 48 hours in
480 total.

481 **Real time PCR**
482 4 day-old wild-type Ler seedlings were immersed into 5mM NAA solution in liquid GM
483 medium, and grown under continuous light without shaking for 15 hours. Cotyledons,
484 hypocotyl, and roots were removed under dissecting scope, and only shoot meristem and
485 the first pair of leaves were collected and immediately frozen in liquid nitrogen. Each
486 biological replicate, represents tissue from 10-15 individual seedlings. Five biological
487 replicates were collected for both mock and NAA treatment. RNeasy Mini kit (Qiagen)
488 was used according to manufacturer's instruction for RNA extraction. 1 microgram of
489 RNA was used for cDNA preparation using Super script III reverse transcriptase for Q-
490 PCR analysis. Q-PCRs were performed in a StepOne Plus Real Time PCR system thermo
491 cycler (The applied bio systems) using 20µl of PCR reaction containing 10 µL of SYBR
492 Green mix (Roche), 1µl of primer mix (10µm), 2µl of 1:10 diluted cDNA and 7 µl of
493 water. Transcript levels were normalized to ACTIN2 transcript levels. Data was analyzed
494 using the $2^{-\Delta\Delta CT}$ method. A freely available online tool was used for analysis using an
495 unpaired t-test of the RT-PCR results: http://graphpad.com/data-analysis-resource-
496 center/. For p-value calculation, data entry format with mean, SD and N was used.
497 Measurements and calculations for all replicates are provided in Table S4.

498 **Model for auxin and PIN1 dynamics**
499 We developed a computational model to understand how interplay between the HD-
500 ZIPIII and KAN pattern and PIN1 dynamics can influence auxin transport and primordia
501 initiation. The model introduces a dependence on KANADI and REVOLUTA into
502 previous models describing PIN1 and auxin dynamics (Bhatia et al., 2016; Heisler et al.,
503 2010; Heisler and Jonsson, 2006; Jonsson et al., 2006; Sahlin et al., 2009). In the model,

504 auxin resides in cell compartments and is able to move between cells either via active
505 transport mediated by PIN1 proteins or passively via a diffusion-like process. PIN1
506 proteins cycle between cytosol and membrane compartments and a quasi-equilibrium
507 model is used for determining its membrane localization at any time point. Auxin
508 generates a signal able to polarise PIN1 in neighboring cells, i.e. a high auxin
509 concentration increases the amount of PIN1 proteins in the neighboring cell membrane
510 facing that cell. The molecule X in our model acts as a mediator of the signalling between
511 auxin and PIN1, and the signal has previously been interpreted as a molecular (Jonsson et
512 al., 2006), or mechanical stress signal (Heisler et al., 2010). In the model, the signal X is
513 activated by auxin, and repressed by KAN and REV. The equations governing the
514 dynamics of the molecules are

515 $$\frac{dA_i}{dt} = c_A - d_A A_i + \frac{1}{V_i}\left[D \sum_{j\in\{N_i\}} a_{ij}\left(A_j - A_i\right) + T \sum_{j\in\{N_i\}} a_{ij}\left(P_{ji}A_j - P_{ij}A_i\right)\right],$$

516 $$\frac{dP_i^{[tot]}}{dt} = c_P - d_P P_i^{[tot]},$$

517 $$\frac{dX_i}{dt} = V_X \frac{A_i^{n_{XA}}}{(K_{XA}^{n_{XA}} + A_i^{n_{XA}})} \frac{K_{XR}^{n_{XR}}}{(K_{XR}^{n_{XR}} + R_i^{n_{XR}})} \frac{K_{XK}^{n_{XK}}}{(K_{XK}^{n_{XK}} + K_i^{n_{XK}})} - d_X X_i,$$

518

519 where A_i is the auxin concentration and X_i is the level of the signalling molecule in cell i.
520 $\{N_i\}$ is the set of cells neighboring cell i, V_i is the cell volume of cell i, and $a_{ij} = a_{ji}$ is the
521 cell wall area for the wall section between cells i and j. $P_i^{[tot]}$ is the total
522 PIN1concentration in the cytosol and membrane compartments of cell i. Membrane-
523 bound PIN1 appears in the equation as P_{ij}, which is the PIN1 concentration in the
524 membrane compartment of cell i that faces cell j. A simple linear feedback between the
525 signal X_j and P_{ij} is used and a quasi-stable assumption, introduced in Jönsson *et. al.*
526 (2006), leads to

527

528 $$P_{ij} = \frac{P_i^{[tot]}[\left(1 - k_p\right) + k_p X_j]}{f_p + \sum_{k\in\{N_i\}}[\left(1 - k_p\right) + k_p X_k]},$$

529

530 where $f_p = k_n/k_x$ is the ratio of endocytosis and exocytosis rates and k_p sets the relation
531 between symmetric and polarized exocytosis ($dP_{ij}/dt = k_x[(1-k_p) + k_p X_j]P_i - k_n P_{ij}$, where
532 P_i is the PIN1 in the cytosol compartment). The feedback between auxin and PIN1 is
533 identical to previous models if the KAN and REV factors in the dX_i/dt equation are 1 (e.g.
534 by setting KAN and REV to zero in all cells), while the polarising signal becomes
535 reduced in regions where KAN and/or REV are expressed. This effect tunes the
536 interaction between the dorsoventral patterning and PIN1/auxin dynamics (cf. Figure. 8B
537 and D).
538 The model was simulated using the in-house developed software organism/tissue
539 (http://dev.thep.lu.se/organism/, available upon request). Files defining the model with
540 parameter values (Suppl. Table S3) and initial configuration of (static) cell geometries
541 and KAN and REV expression domains are provided as Supplemental Information. The
542 simulations use a 5th order Runge-Kutta solver with adaptive step size (William H. Press,
543 2007), and initial auxin, PIN1 and X concentrations are set to zero in all compartments.
544
545 **Generation of geometrical template**
546 The model defined above was run on a template containing a predefined KAN/REV
547 pattern (provided as Supplemental material file, Figure. 8C). The geometry of the
548 template was generated by a combination of cell/wall growth and mechanical interactions
549 together with a shortest path division rule (Sahlin and Jonsson, 2010). A KAN/REV
550 pattern was generated by the equations
551

552 $$\frac{dK_i}{dt} = V_K \frac{r_i^{n_K}}{K_K^{n_K} + r_i^{n_K}} - d_K K_i,$$

553 $$\frac{dR_i}{dt} = V_R \frac{r_i^{n_R}}{K_R^{n_R} + r_i^{n_R}} - d_R R_i.$$

554
555 This system was run to equilibrium on the above-mentioned template. In the above
556 equations r_i is the distance of cell i from the center of the template. The parameters were
557 set to V_K=V_R=d_K=d_R=1, K_K=30, K_R=25, n_K=n_R=20. These parameters are set such that
558 two distinct domains are created, with a small overlap of low KAN and REV

559 concentrations in the boundary between these regions. To make the transition of KAN
560 concentrations between domains sharper, KAN concentrations were set to 0 (1) if $K_i \leq 0.5$
561 (>0.5).
562
563
564 **Acknowledgements**
565 We thank M. E. Byrne for helpful feedback and ideas on the manuscript. We thank J.
566 Bowman for helpful discussions as well as for plasmids containing REVr and PHVr
567 cDNAs. We thank D. Weijers and C. Y. Liao for a plasmid containing
568 pDR5v2::ntdTomato; K. Nakajima for the T-DNA construct of miR166Ap::GFPER, Dr
569 Atsushi Miyawaki from RIKEN Brain Science Institute for the VENUS fluorescent
570 protein which was obtained through an MTA. The E.M.M. laboratory is supported by
571 funds from the Howard Hughes Medical Institute and the Gordon and Betty Moore
572 Foundation (through grant GBMF3406). The research leading to these results received
573 funding from the Australian Research Council (M.G.H.) and European Research Council
574 under the European Union's Seventh Framework Programme (FP/2007-2013) / ERC
575 Grant Agreement n. 261081 (M.G.H.), as well as the People Programme (Marie Curie
576 Actions) under REA grant agreement n. 255089 (P.S.). The work was also supported by:
577 the European Molecular Biology Laboratory (X.Y., M.P.C., C.O., P.S, N.B., H.R. and
578 M.G.H.); the EMBL International PhD Programme (X.Y., N.B. and M.P.C.); Gatsby
579 Charitable Foundation (GAT3395/PR4) (H.J) and Swedish Research Council (VR2013-
580 4632) (H.J). The authors declare no competing financial interests. Supplement contains
581 additional data and movie. We declare there are no competing interests.
582
583
584
585
586 **References**
587
588 **Barrell, P. J. and Conner, A. J.** (2006). Minimal T-DNA vectors suitable for
589 agricultural deployment of transgenic plants. *Biotechniques* **41**, 708-710.

590 **Bhatia, N., Bozorg, B., Larsson, A., Ohno, C., Jonsson, H. and Heisler, M. G.** (2016).
591 Auxin Acts through MONOPTEROS to Regulate Plant Cell Polarity and Pattern
592 Phyllotaxis. *Curr Biol* **26**, 3202-3208.
593 **Bilsborough, G. D., Runions, A., Barkoulas, M., Jenkins, H. W., Hasson, A.,**
594 **Galinha, C., Laufs, P., Hay, A., Prusinkiewicz, P. and Tsiantis, M.** (2011).
595 Model for the regulation of Arabidopsis thaliana leaf margin development. *Proc*
596 *Natl Acad Sci U S A* **108**, 3424-3429.
597 **Craft, J., Samalova, M., Baroux, C., Townley, H., Martinez, A., Jepson, I., Tsiantis,**
598 **M. and Moore, I.** (2005). New pOp/LhG4 vectors for stringent glucocorticoid-
599 dependent transgene expression in Arabidopsis. *Plant J.* **41**, 899-918.
600 **de Reuille, P. B., Bohn-Courseau, I., Ljung, K., Morin, H., Carraro, N., Godin, C.**
601 **and Traas, J.** (2006). Computer simulations reveal properties of the cell-cell
602 signaling network at the shoot apex in Arabidopsis. *Proc Natl Acad Sci U S A*
603 **103**, 1627-1632.
604 **Emery, J. F., Floyd, S. K., Alvarez, J., Eshed, Y., Hawker, N. P., Izhaki, A., Baum,**
605 **S. F. and Bowman, J. L.** (2003). Radial patterning of Arabidopsis shoots by class
606 III HD-ZIP and KANADI genes. *Curr Biol* **13**, 1768-1774.
607 **Gleave, A. P.** (1992). A Versatile Binary Vector System with a T-DNA Organizational-
608 Structure Conducive to Efficient Integration of Cloned DNA into the Plant
609 Genome. *Plant Molecular Biology* **20**, 1203-1207.
610 **Gordon, S. P., Heisler, M. G., Reddy, G. V., Ohno, C., Das, P. and Meyerowitz, E.**
611 **M.** (2007). Pattern formation during de novo assembly of the Arabidopsis shoot
612 meristem. *Development* **134**, 3539-3548.
613 **Hagemann, W. and Gleissberg, S.** (1996). Organogenetic capacity of leaves: The
614 significance of marginal blastozones in angiosperms. *Plant Syst. Evol.* **199**, 121-
615 152.
616 **Hayashi, K., Neve, J., Hirose, M., Kuboki, A., Shimada, Y., Kepinski, S. and Nozaki,**
617 **H.** (2012). Rational design of an auxin antagonist of the SCF(TIR1) auxin
618 receptor complex. *ACS chemical biology* **7**, 590-598.
619 **He, W., Brumos, J., Li, H., Ji, Y., Ke, M., Gong, X., Zeng, Q., Li, W., Zhang, X., An,**
620 **F., et al.** (2011). A small-molecule screen identifies L-kynurenine as a
621 competitive inhibitor of TAA1/TAR activity in ethylene-directed auxin
622 biosynthesis and root growth in Arabidopsis. *Plant Cell* **23**, 3944-3960.
623 **Heisler, M. G., Hamant, O., Krupinski, P., Uyttewaal, M., Ohno, C., Jonsson, H.,**
624 **Traas, J. and Meyerowitz, E. M.** (2010). Alignment between PIN1 polarity and
625 microtubule orientation in the shoot apical meristem reveals a tight coupling
626 between morphogenesis and auxin transport. *PLoS Biol* **8**, e1000516.
627 **Heisler, M. G. and Jonsson, H.** (2006). Modeling auxin transport and plant
628 development. *Journal of Plant Growth Regulation* **25**, 302-312.
629 **Heisler, M. G. and Ohno, C.** (2014). Live-imaging of the Arabidopsis inflorescence
630 meristem. In *Flower Development*, pp. 431-440: Springer.
631 **Heisler, M. G., Ohno, C., Das, P., Sieber, P., Reddy, G. V., Long, J. A. and**
632 **Meyerowitz, E. M.** (2005). Patterns of auxin transport and gene expression
633 during primordium development revealed by live imaging of the Arabidopsis
634 inflorescence meristem. *Current Biology* **15**, 1899-1911.

635 **Huang, T., Harrar, Y., Lin, C., Reinhart, B., Newell, N. R., Talavera-Rauh, F.,**
636 **Hokin, S. A., Barton, M. K. and Kerstetter, R. A.** (2014). Arabidopsis
637 KANADI1 acts as a transcriptional repressor by interacting with a specific cis-
638 element and regulates auxin biosynthesis, transport, and signaling in opposition to
639 HD-ZIPIII factors. *Plant Cell* **26**, 246-262.
640 **Husbands, A. Y., Chitwood, D. H., Plavskin, Y. and Timmermans, M. C.** (2009).
641 Signals and prepatterns: new insights into organ polarity in plants. *Genes Dev* **23**,
642 1986-1997.
643 **Izhaki, A. and Bowman, J. L.** (2007). KANADI and class III HD-Zip gene families
644 regulate embryo patterning and modulate auxin flow during embryogenesis in
645 Arabidopsis. *Plant Cell* **19**, 495-508.
646 **Jonsson, H., Heisler, M. G., Shapiro, B. E., Meyerowitz, E. M. and Mjolsness, E.**
647 (2006). An auxin-driven polarized transport model for phyllotaxis. *Proceedings of*
648 *the National Academy of Sciences of the United States of America* **103**, 1633-
649 1638.
650 **Karimi, M., Inze, D. and Depicker, A.** (2002). GATEWAY vectors for Agrobacterium-
651 mediated plant transformation. *Trends Plant Sci* **7**, 193-195.
652 **Kerstetter, R. A., Bollman, K., Taylor, R. A., Bomblies, K. and Poethig, R. S.** (2001).
653 KANADI regulates organ polarity in Arabidopsis. *Nature* **411**, 706-709.
654 **Kidner, C. A. and Martienssen, R. A.** (2004). Spatially restricted microRNA directs
655 leaf polarity through ARGONAUTE1. *Nature* **428**, 81-84.
656 **Koenig, D., Bayer, E., Kang, J., Kuhlemeier, C. and Sinha, N.** (2009). Auxin patterns
657 Solanum lycopersicum leaf morphogenesis. *Development* **136**, 2997-3006.
658 **Kuhlemeier, C. and Timmermans, M. C.** (2016). The Sussex signal: insights into leaf
659 dorsiventrality. *Development* **143**, 3230-3237.
660 **Landrein, B., Kiss, A., Sassi, M., Chauvet, A., Das, P., Cortizo, M., Laufs, P.,**
661 **Takeda, S., Aida, M., Traas, J., et al.** (2015). Mechanical stress contributes to
662 the expression of the STM homeobox gene in Arabidopsis shoot meristems. *eLife*
663 **4**, e07811.
664 **Liao, C. Y., Smet, W., Brunoud, G., Yoshida, S., Vernoux, T. and Weijers, D.** (2015).
665 Reporters for sensitive and quantitative measurement of auxin response. *Nat*
666 *Methods* **12**, 207-210, 202 p following 210.
667 **McConnell, J. R., Emery, J., Eshed, Y., Bao, N., Bowman, J. and Barton, M. K.**
668 (2001). Role of PHABULOSA and PHAVOLUTA in determining radial
669 patterning in shoots. *Nature* **411**, 709-713.
670 **Merelo, P., Ram, H., Pia Caggiano, M., Ohno, C., Ott, F., Straub, D., Graeff, M.,**
671 **Cho, S. K., Yang, S. W., Wenkel, S., et al.** (2016). Regulation of MIR165/166
672 by class II and class III homeodomain leucine zipper proteins establishes leaf
673 polarity. *Proc Natl Acad Sci U S A*.
674 **Merelo, P., Xie, Y., Brand, L., Ott, F., Weigel, D., Bowman, J. L., Heisler, M. G. and**
675 **Wenkel, S.** (2013). Genome-wide identification of KANADI1 target genes. *PLoS*
676 *One* **8**, e77341.
677 **Miyashima, S., Honda, M., Hashimoto, K., Tatematsu, K., Hashimoto, T., Sato-**
678 **Nara, K., Okada, K. and Nakajima, K.** (2013). A comprehensive expression
679 analysis of the Arabidopsis MICRORNA165/6 gene family during embryogenesis

680 reveals a conserved role in meristem specification and a non-cell-autonomous
681 function. *Plant Cell Physiol* **54**, 375-384.
682 **Miyashima, S., Koi, S., Hashimoto, T. and Nakajima, K.** (2011). Non-cell-
683 autonomous microRNA165 acts in a dose-dependent manner to regulate multiple
684 differentiation status in the Arabidopsis root. *Development* **138**, 2303-2313.
685 **Nagai, T., Ibata, K., Park, E. S., Kubota, M., Mikoshiba, K. and Miyawaki, A.**
686 (2002). A variant of yellow fluorescent protein with fast and efficient maturation
687 for cell-biological applications. *Nature Biotechnology* **20**, 87-90.
688 **Nakata, M., Matsumoto, N., Tsugeki, R., Rikirsch, E., Laux, T. and Okada, K.**
689 (2012). Roles of the middle domain-specific WUSCHEL-RELATED
690 HOMEOBOX genes in early development of leaves in Arabidopsis. *Plant Cell* **24**,
691 519-535.
692 **Nguyen, A. W. and Daugherty, P. S.** (2005). Evolutionary optimization of fluorescent
693 proteins for intracellular FRET. *Nat Biotechnol* **23**, 355-360.
694 **Nishimura, T., Hayashi, K., Suzuki, H., Gyohda, A., Takaoka, C., Sakaguchi, Y.,**
695 **Matsumoto, S., Kasahara, H., Sakai, T., Kato, J., et al.** (2014). Yucasin is a
696 potent inhibitor of YUCCA, a key enzyme in auxin biosynthesis. *Plant J* **77**, 352-
697 366.
698 **Nogueira, F. T. S., Madi, S., Chitwood, D. H., Juarez, M. T. and Timmermans, M.**
699 **C. P.** (2007). Two small regulatory RNAs establish opposing fates of a
700 developmental axis. *Genes & Development* **21**, 750-755.
701 **Otsuga, D., DeGuzman, B., Prigge, M. J., Drews, G. N. and Clark, S. E.** (2001).
702 REVOLUTA regulates meristem initiation at lateral positions. *Plant J* **25**, 223-
703 236.
704 **Qi, J., Wang, Y., Yu, T., Cunha, A., Wu, B., Vernoux, T., Meyerowitz, E. and Jiao,**
705 **Y.** (2014). Auxin depletion from leaf primordia contributes to organ patterning.
706 *Proc Natl Acad Sci U S A* **111**, 18769-18774.
707 **Reinhardt, D., Frenz, M., Mandel, T. and Kuhlemeier, C.** (2005). Microsurgical and
708 laser ablation analysis of leaf positioning and dorsoventral patterning in tomato.
709 *Development* **132**, 15-26.
710 **Reinhardt, D., Mandel, T. and Kuhlemeier, C.** (2000). Auxin regulates the initiation
711 and radial position of plant lateral organs. *Plant Cell* **12**, 507-518.
712 **Reinhardt, D., Pesce, E. R., Stieger, P., Mandel, T., Baltensperger, K., Bennett, M.,**
713 **Traas, J., Friml, J. and Kuhlemeier, C.** (2003). Regulation of phyllotaxis by
714 polar auxin transport. *Nature* **426**, 255-260.
715 **Roslan, H. A., Salter, M. G., Wood, C. D., White, M. R., Croft, K. P., Robson, F.,**
716 **Coupland, G., Doonan, J., Laufs, P., Tomsett, A. B., et al.** (2001).
717 Characterization of the ethanol-inducible alc gene-expression system in
718 Arabidopsis thaliana. *Plant J* **28**, 225-235.
719 **Rosso, M. G., Li, Y., Strizhov, N., Reiss, B., Dekker, K. and Weisshaar, B.** (2003). An
720 Arabidopsis thaliana T-DNA mutagenized population (GABI-Kat) for flanking
721 sequence tag-based reverse genetics. *Plant Mol Biol* **53**, 247-259.
722 **Sahlin, P. and Jonsson, H.** (2010). A modeling study on how cell division affects
723 properties of epithelial tissues under isotropic growth. *PLoS One* **5**, e11750.

724 **Sahlin, P., Soderberg, B. and Jonsson, H.** (2009). Regulated transport as a mechanism
725 for pattern generation: capabilities for phyllotaxis and beyond. *J Theor Biol* **258**,
726 60-70.
727 **Samalova, M., Brzobohaty, B. and Moore, I.** (2005). pOp6/LhGR: a stringently
728 regulated and highly responsive dexamethasone-inducible gene expression system
729 for tobacco. *Plant J.* **41**, 919-935.
730 **Sessions, A., Weigel, D. and Yanofsky, M. F.** (1999). The Arabidopsis thaliana
731 MERISTEM LAYER 1 promoter specifies epidermal expression in meristems and
732 young primordia. *Plant J* **20**, 259-263.
733 **Shaner, N. C., Campbell, R. E., Steinbach, P. A., Giepmans, B. N., Palmer, A. E. and**
734 **Tsien, R. Y.** (2004). Improved monomeric red, orange and yellow fluorescent
735 proteins derived from Discosoma sp. red fluorescent protein. *Nat Biotechnol* **22**,
736 1567-1572.
737 **Shimizu, R., Ji, J., Kelsey, E., Ohtsu, K., Schnable, P. S. and Scanlon, M. J.** (2009).
738 Tissue specificity and evolution of meristematic WOX3 function. *Plant Physiol.*
739 **149**, 841-850.
740 **Smith, R. S., Guyomarc'h, S., Mandel, T., Reinhardt, D., Kuhlemeier, C. and**
741 **Prusinkiewicz, P.** (2006). A plausible model of phyllotaxis. *Proc Natl Acad Sci*
742 *U S A* **103**, 1301-1306.
743 **Smith, Z. R. and Long, J. A.** (2010). Control of Arabidopsis apical-basal embryo
744 polarity by antagonistic transcription factors. *Nature* **464**, 423-426.
745 **Snow, M. and Snow, R.** (1959). The dorsiventrality of leaf primordia. *New Phytol.* **58**,
746 188-207.
747 **Snow, M. S., R.** (1931). Experiments on phyllotaxis. I. The effect of isolating a
748 primordium. *Philos Trans R Soc Lond B Biol Sci* **221**, 1-43.
749 **Sussex, I. M.** (1951). Experiments on the cause of dorsiventrality in leaves. *Nature* **167**,
750 651-652.
751 **----** (1955). Morphogenesis in Solanum tuberosum I: experimental investigation of leaf
752 dorsiventrality and orientation in the juvenile shoot. *Phytomorphology* **5**, 286-300.
753 **Tameshige, T., Fujita, H., Watanabe, K., Toyokura, K., Kondo, M., Tatematsu, K.,**
754 **Matsumoto, N., Tsugeki, R., Kawaguchi, M., Nishimura, M., et al.** (2013).
755 Pattern dynamics in adaxial-abaxial specific gene expression are modulated by a
756 plastid retrograde signal during Arabidopsis thaliana leaf development. *PLoS*
757 *Genet* **9**, e1003655.
758 **William H. Press, S. A. T., William T. Vetterling, Brian P. Flannery** (2007).
759 *Numerical Recipes: The art of scientific computing* (3rd edn). New York, NY,
760 USA: Cambridge University Press
761 **Yan, J., Gu, Y., Jia, X., Kang, W., Pan, S., Tang, X., Chen, X. and Tang, G.** (2012).
762 Effective small RNA destruction by the expression of a short tandem target mimic
763 in Arabidopsis. *Plant Cell* **24**, 415-427.
764 **Yao, X., Wang, H., Li, H., Yuan, Z., Li, F., Yang, L. and Huang, H.** (2009). Two
765 types of cis-acting elements control the abaxial epidermis-specific transcription of
766 the MIR165a and MIR166a genes. *FEBS Lett* **583**, 3711-3717.
767 **Zhang, Z., Tucker, E., Hermann, M. and Laux, T.** (2017). A Molecular Framework
768 for the Embryonic Initiation of Shoot Meristem Stem Cells. *Dev Cell* **40**, 264-277
769 e264.

770 **Zuo, J., Niu, Q. W., Moller, S. G. and Chua, N. H.** (2001). Chemical-regulated, site-
771 specific DNA excision in transgenic plants. *Nat Biotechnol* **19**, 157-161.
772

773
774
775
776

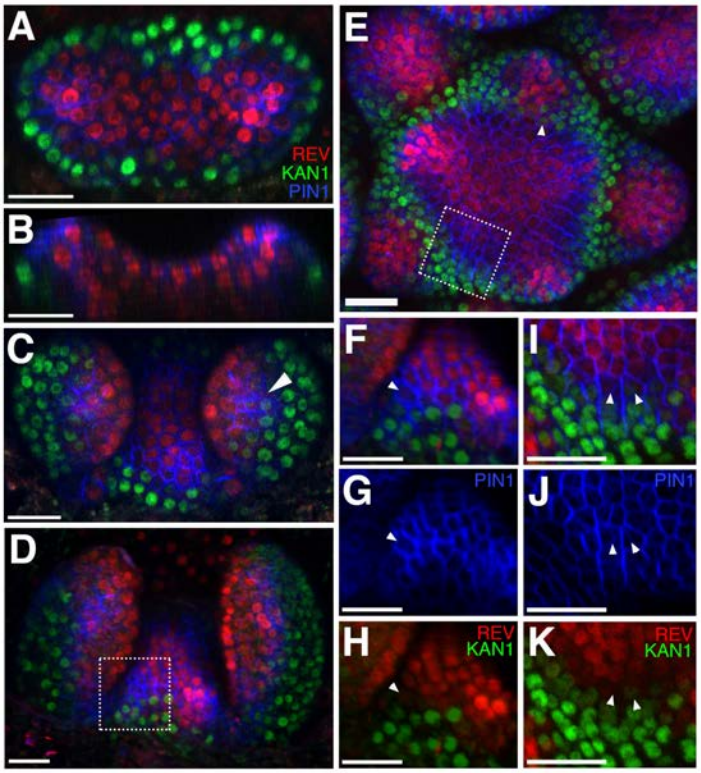

Figure 1.

Organ initiation is centered on a boundary between the expression domains of genes involved in leaf dorsoventrality.

(**A to D**) Confocal projections showing REV-2×YPet (red), PIN1-CFP (blue) and KAN1-2×GFP (green) expression in a vegetative shoot apical meristem at 3 days (A), 4 days (C) and 5 days (D) after stratification (DAS), respectively. (B) Longitudinal reconstructed section of seedling shown in (A). Dashed box in (D) corresponds to close up in (F) to (H). (**E**) Expression pattern of REV-2×YPet, KAN1-2×GFP and PIN1-CFP in an inflorescence meristem. Dashed box corresponds to close ups in (I) to (K). White arrow head marks region where KAN1-2×GFP expression is being reestablished after organ emergence. (**F to K**) localized PIN1-CFP expression marking organ inception at the REV-2×YPet /KAN1-2×GFP boundary in both the vegetative meristem (F) to (H) and inflorescence meristem (I) to (K). White arrow heads mark cells in between the REV-2×YPet and KAN1-2×GFP expression domains where PIN1-CFP expression is highest. Scale bars represent 20 μm.

795

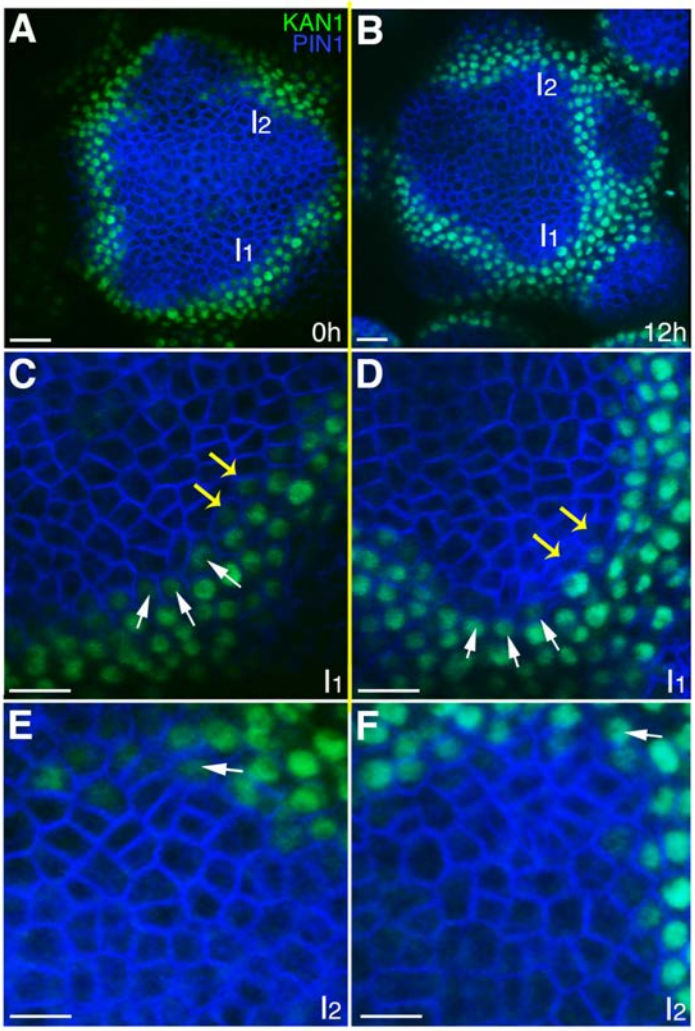

796
797 **Figure 2.**
798 **The expression of KAN1-2×GFP is relatively stable with respect to the underlying**
799 **cells within initiating organs.**
800 **(A-B)** Confocal projections showing an inflorescence meristem viewed from above
801 expressing PIN1-CFP (blue) and KAN1-2×GFP (green) at two time points (0h and 12h).
802 Two incipient primordia are marked I1 and I2. **(C-D)** Close up views corresponding to
803 primordium I1 from (A) and (B) with white arrows marking three cells at the edge of
804 KAN1-2×GFP expression that retain this expression over the time interval. Yellow
805 arrows mark two cells in which KAN1-2×GFP is absent at 12h. **(E)** Close up views
806 corresponding to primordium I2 from (A) and (B) with white arrows marking three cells
807 that retain KAN1-2×GFP expression at the adaxial (towards the meristem) edge over the
808 time interval. Bars represent 20 μm in (A) and (B); 10 μm in (C) to (F).

809
810

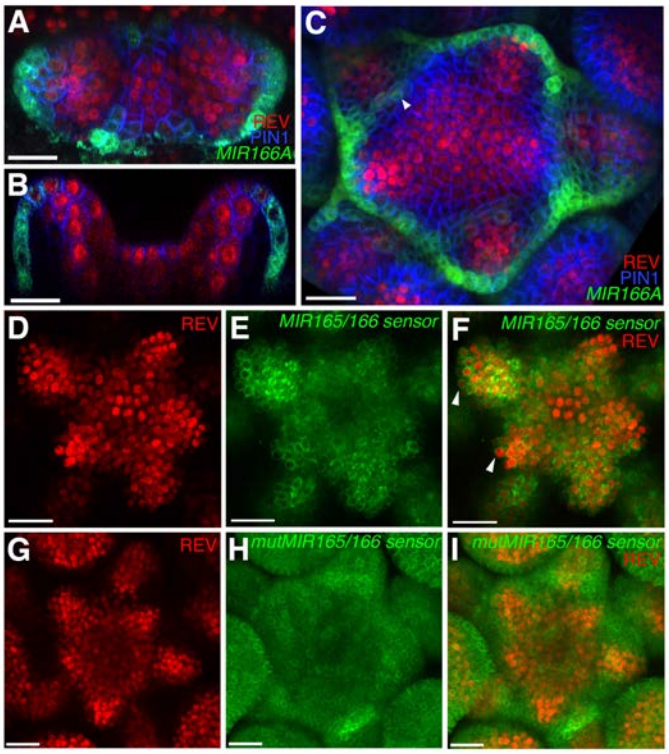

811

812 **Figure 3.**

813 **Expression and activity of MIR165/166 is localized to the periphery of the shoot**
814 **meristem.**

815 **(A)** Expression of *MIR166Ap::GFPER* (green), PIN1-CFP (blue) and REV-2×YPet (red)
816 in the vegetative meristem (VM) at 3.5 DAS. **(B)** Longitudinal section of meristem
817 shown in (A). **(C)** Expression of *MIR166Ap::GFPER* (green), PIN1-CFP (blue) and
818 REV-2×YPet (red) in the inflorescence meristem (IM). White arrow head marks the
819 reestablishment of *MIR166Ap::GFPER* expression around the meristem after organ
820 emergence. **(D to F)** Expression of REV-2×YPet (red) alone (D), a MIR165/166
821 biosensor driven by the *UBQ10* promoter (green) alone (E) and both combined in the
822 same IM (F). (**G to I**) Corresponding control for (D to F) where the MIR165/166
823 biosensor has been rendered insensitive to MIRNA activity. Bars represent 20 μm.

824

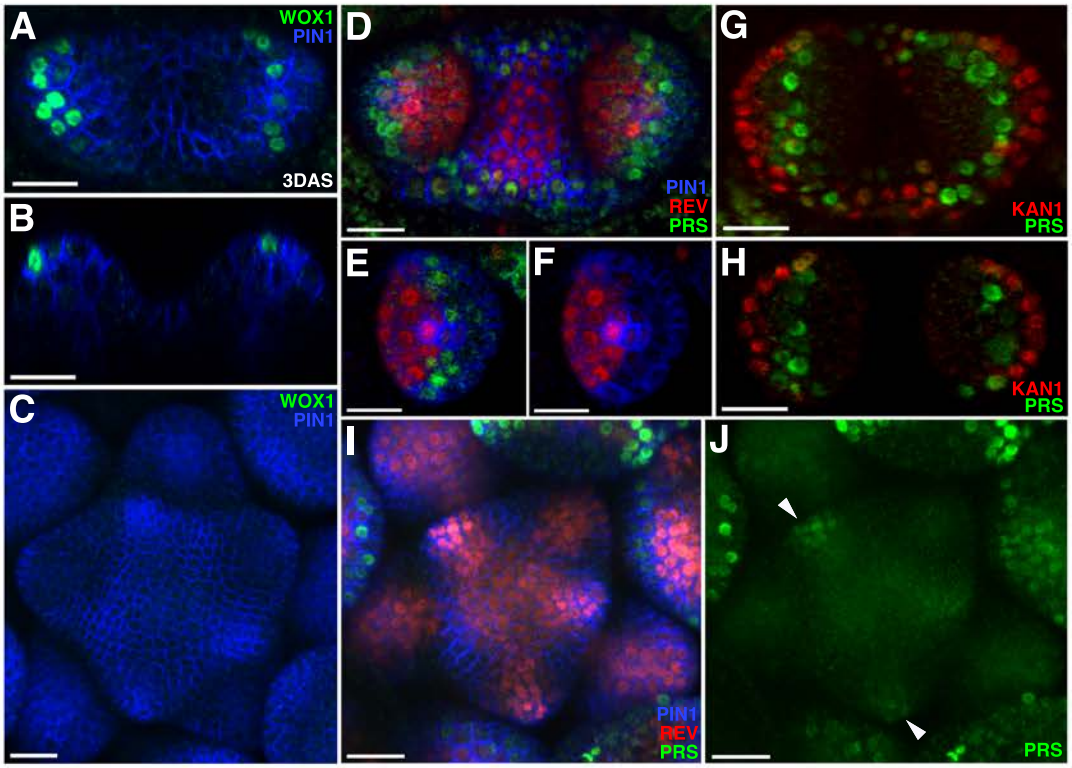

825

826 **Figure 4.**

827 **Expression patterns of 2×GFP-WOX1 and PRS-2×GFP**

828 (**A**) Confocal projections showing PIN1-CFP (blue) and 2×GFP-WOX1 (green)
829 expression patterns in the vegetative meristem and leaves of seedlings at 3 DAS. (**B**)
830 Longitudinal section of meristem shown in (A). (**C**) An inflorescence meristem image
831 showing 2×GFP-WOX1 is not expressed in the IM. (**D**) Confocal projection showing
832 PIN1-CFP (blue), PRS-2×GFP (green) and REV-2×YPet (red) expression in the
833 vegetative meristem and leaves at 3.5 DAS, where PRS-2×GFP is expressed surrounding
834 the VM and along the leaf margins. (**E and F**) Cross sections of leaf on the right side in
835 (D) showing the expression of PRS-2×GFP in the middle domain of the leaf. (**G and H**)
836 Confocal projection and cross section showing PRS-2×GFP (green) and KAN1-2×CFP
837 (red) expression patterns in the vegetative meristem and leaves of seedlings at 3 DAS. **(I**
838 **and J)** PRS-2×GFP (green) is expressed in the young flower primodia in the IM,
839 indicated with arrowhead in (J). Bar = 20 μm.

840

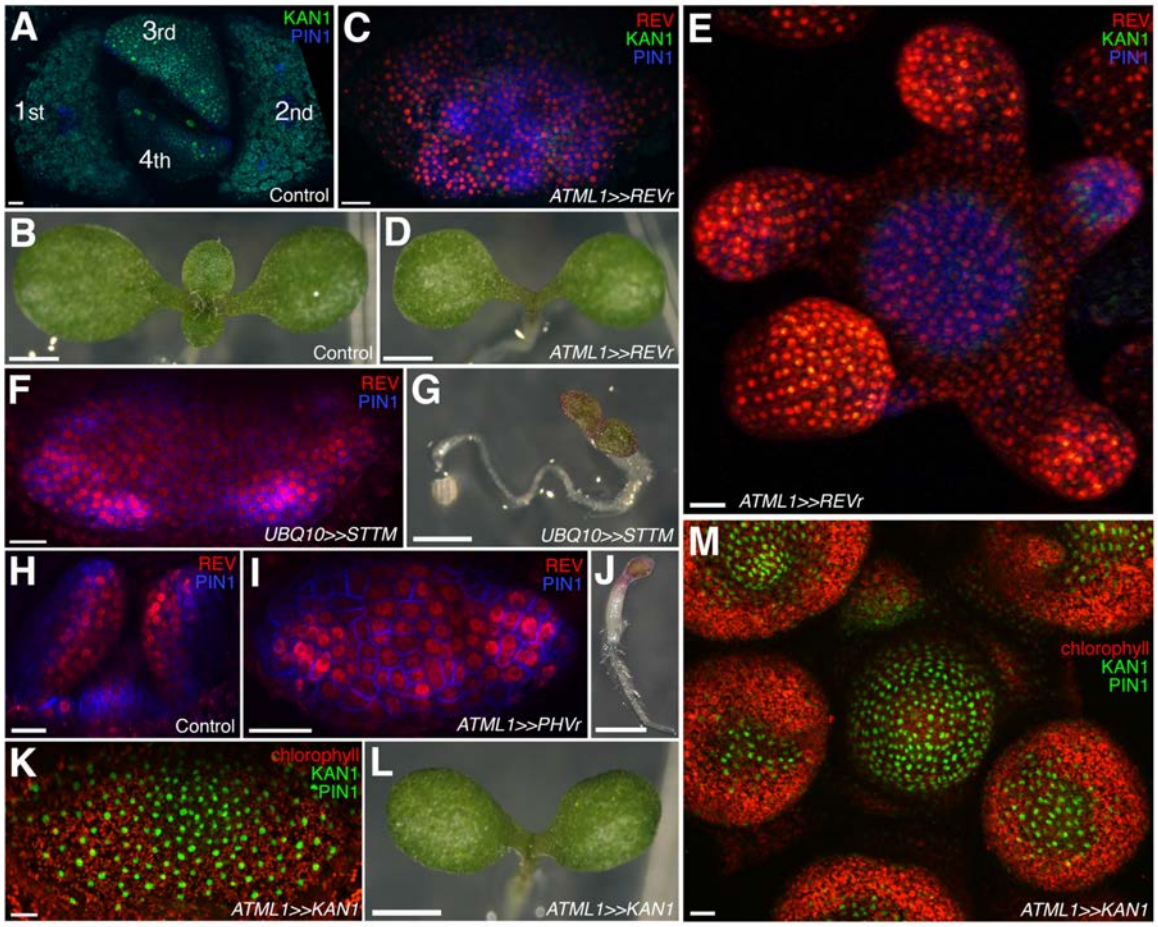

Figure 5.

Organ initiation depends on the restriction of Class III HD-ZIP and KANADI expression in the shoot.

(**A**) Confocal projection showing wild type control seedling at 7DAS viewed from above for comparison to (C) and (F). **(B)** Macroscopic view of control seedling at 7DAS for comparison to (D), (G) and (L). (**C**) Arrest of organogenesis after ectopic expression of REVr-2×VENUS from the *ATML1* promoter in the vegetative meristem (7 DAS) after germination on DEX, KAN1-2×GFP (green) expression is down regulated and could only be detected in a few cells in the sub-epidermis. Although PIN1-CFP (blue) expression is patchy, no leaves developed. **(D)** Macroscopic view of plant in (C). (**E**) Arrest of organogenesis after ectopic expression of REVr-2×VENUS (red) from the *ATML1* in the IM after 3 DEX treatments over 6 days. Note the absence of KAN1-2×GFP signal. **(F)** Seedlings at 7DAS showing similar phenotype to (C) after induction of a short tandem target mimic (STTM) designed to down regulate MIR165/166 activity. **(G)** Macroscopic

856 view of plant in (F). **(H to J)** Ectopic expression of REV-2YPet (red) and arrest of
857 organogenesis (PIN1-CFP in blue) in 4DAS seedling after induction of MIR165/166
858 resistant PHAVOLUTA. (H) Longitudinal view of uninduced control. Top view (I), and
859 macroscopic view (J) of induced seedling showing arrest of organ development. **(K and**
860 **L)** Confocal projection (K) and macroscopic view (L) of seedling at 7DAS after
861 induction of KAN1-GFP (green) in the epidermis. No leaves have developed
862 (autofluorescence shown in red). (**M**) Arrest of organogenesis after induction of KAN1-
863 GFP (green) driven by the *ATML1* promoter in the IM after 3 DEX treatments over 6
864 days; autofluorescence (red). Bars represent 20 µm in A, C, E, F, H to I, K and M; 1mm
865 in B, D, G, J and L.
866

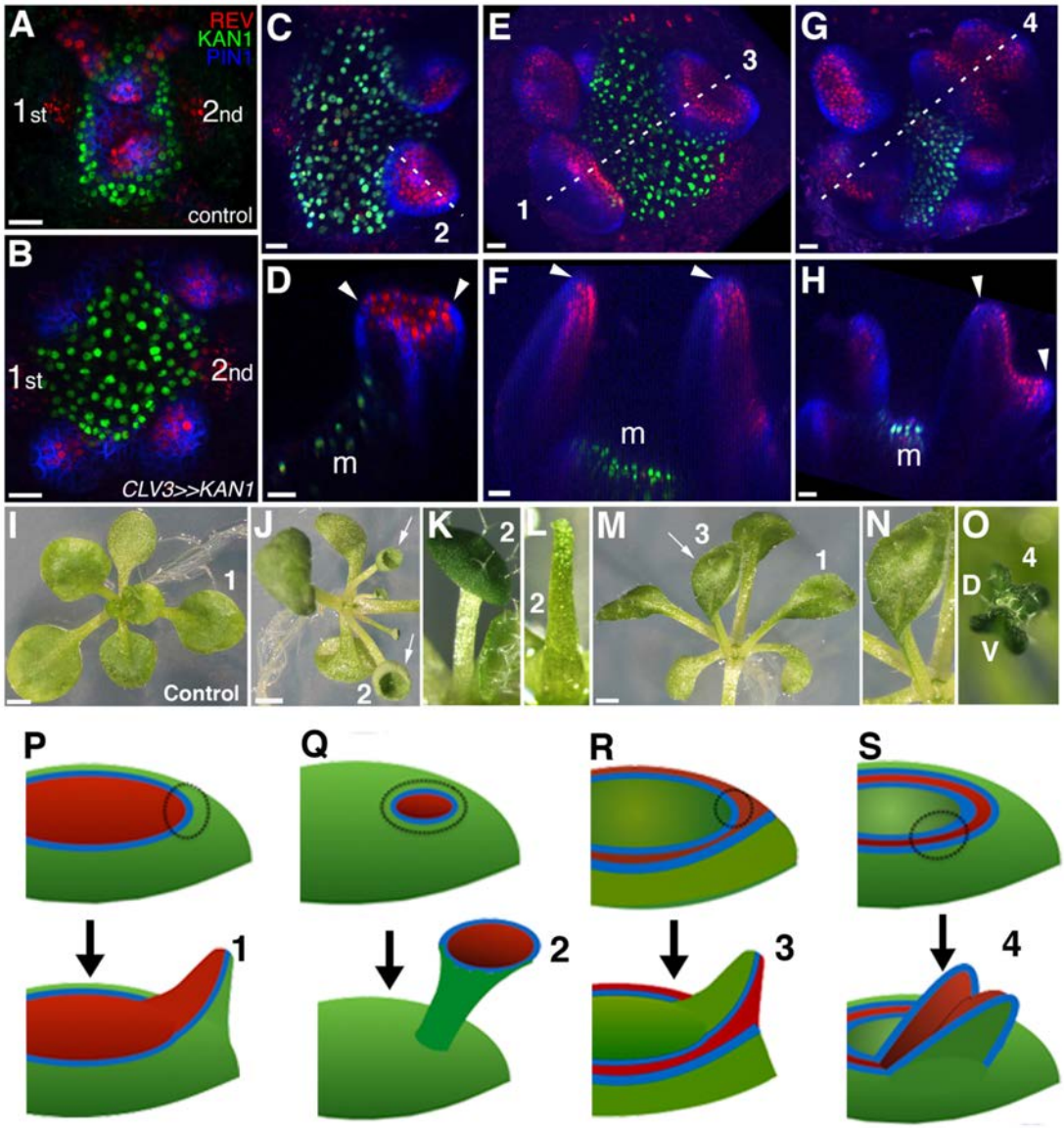

Figure 6.

KANADI1 expression boundaries in the shoot specify organ position and orientation.

(**A and B**) Confocal projections showing organ initiation marked by REV-2×YPet (red) and PIN1-CFP (blue) at border of KAN1-2×GFP expression (green) in wild type (A) and after induction of KAN1-2×GFP using the *CLV3* promoter (B). Distance separating opposite organs was greater for induced (B) compared to control (A) (114.3 ±3.3 µm, n=19 vs 54.2±1.0 µm n=10 (mean±SE, $p<0.05$, t-test)). **(C to H)** Confocal projections (C, E and G) and longitudinal reconstructions corresponding to dashed lines (D, F and H respectively) showing restricted REV-2×YPet expression (red) after ectopic KAN1-

878 2×GFP induction (green). Regions in which neither REV-2×YPet nor KAN1-2×GFP
879 signal was detected may potentially express endogenous KAN1, which was not
880 monitored. Four main configurations of REV expression and morphology were observed
881 (labeled 1 to 4). Class 1 organs (E and F) correspond to the wild type, Class 2 (C and D)
882 express REV-2×YPet centrally, Class 3 (E and F) express REV-2×YPet in a reversed
883 orientation and Class 4 (G and H) express REV-2×YPet centrally and laterally only.
884 Correspondence between REV-2×YPet expression boundaries and leaf margins indicated
885 by arrowheads in D, F and H; m indicates meristem**.** Gamma value changed to highlight
886 PIN1-CFP expression (blue) in (C) to (H). **(I to O)** Examples of mature leaves
887 corresponding to Classes 1 to 4, including the WT (I), cup-shaped (J), lotus-shaped (a
888 variation of cup-shaped) (K), needle-like (a further decrease in extent of dorsal tissue
889 compare to cup-shaped) (L), inverted (M and N) and four bladed (O). "D and V"
890 represent "dorsal" and "ventral" respectively in (O). **(P to S)** Diagrams summarizing
891 proposed configurations of REV and KAN (green) gene expression in leaf founder cells
892 (dashed circles) (upper diagram) leading to the observed phenotypic classes of leaf shape
893 (numbered 1 to 4) (lower diagram) after induction of KAN1-2×GFP using the *CLV3*
894 promoter. (P) represents the wild type Class 1 configuration, (Q) represents Class 2, (R)
895 represents Class 3 and (S) represents Class 4. Scale bars = 20μm in A to H; 1 mm in I, J
896 and M.
897

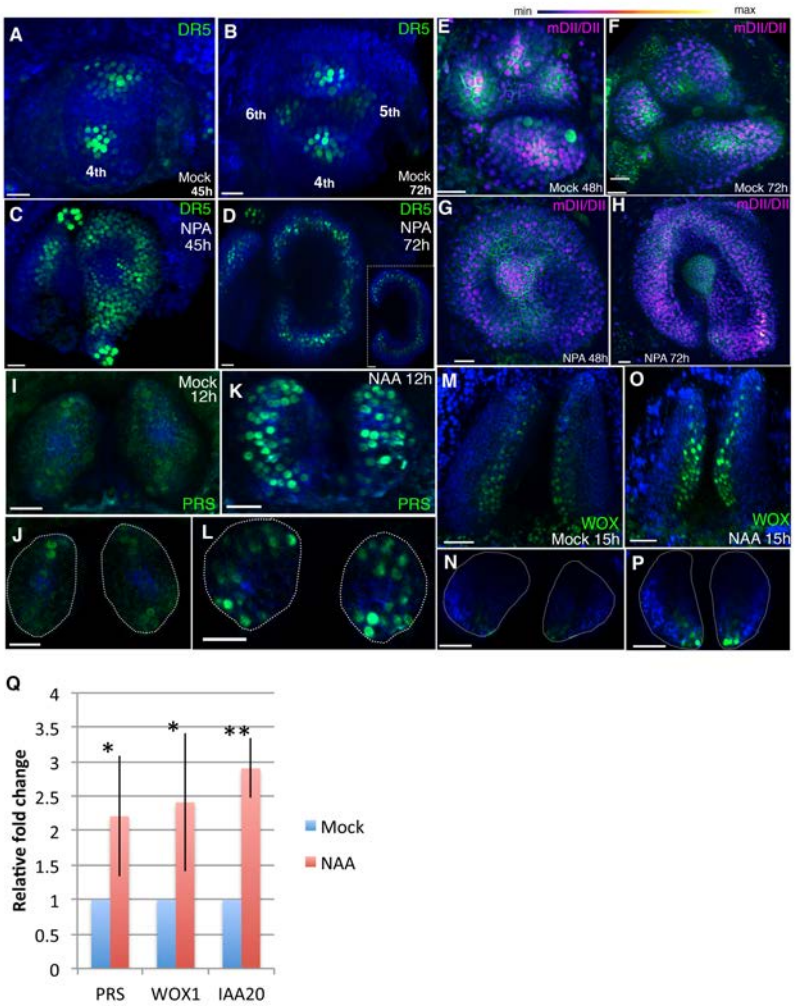

Figure 7.

Auxin promotes PRS and WOX expression.

(A-D) Response of pDR5V2-3×VENUS-N7 (green) auxin transcriptional reporter to NPA in Arabidopsis seedlings 4DAS (Days after Stratification). (A and B) Confocal projections 45 hours (A) and 72 hours (B) after treatment with mock solution. (C and D) Confocal projections 45 hours (C) and 72 hours (D) after treatment with 100μM NPA solution (n=5/5). Inset in (D) shows transverse optical section through the ring-shaped organ showing most DR5 expression localized in the center of the organ. **(E-H)** Expression and response of R2D2 (magenta) to auxin along with PIN1-GFP expression (green) in Arabidopsis seedlings 4DAS. (E and F) Confocal projections 48 hours (E) and 72 hours (F) after treatment with mock solution. (G and H) Confocal projections 48 hours

911 (G) and 72 hours (H) after treatment with 100μM NPA solution (n=4/4). **(I-L)** Expression
912 and response of pPRS::2×GFP-PRS to auxin in Arabidopsis seedlings. Confocal
913 projections and transverse optical slices of seedlings 4DAS showing pPRS::2×GFP-PRS
914 expression (green) 12 hours after treatment with mock solution (I and J) and 5mM NAA
915 (K and L) (n=5/5). **(M-P)** Expression and response of 2XGFP-WOX to auxin in
916 Arabidopsis seedlings. (M and N) Confocal projections (M and O) and corresponding
917 optical slices (N and P) of seedlings 4DAS showing pWOX1::2×GFP-WOX1 expression
918 (green) 12 hours after treatment with mock solution (M and N) and 5mM NAA (O and
919 P). Note WOX expression increases but does not expands beyond its regular expression
920 domain upon auxin addition (n=5/5). **(Q)** Q-PCR analysis of PRS, WOX1 and positive
921 control IAA20 transcripts after 5mM NAA or mock treatment on 4 days old wild-type
922 (Ler) seedlings. *=p<0.05, ***=p<0.001. Scale bars 20μm (A-L, K); 15μm (J and L);
923 30μm (M-P).
924

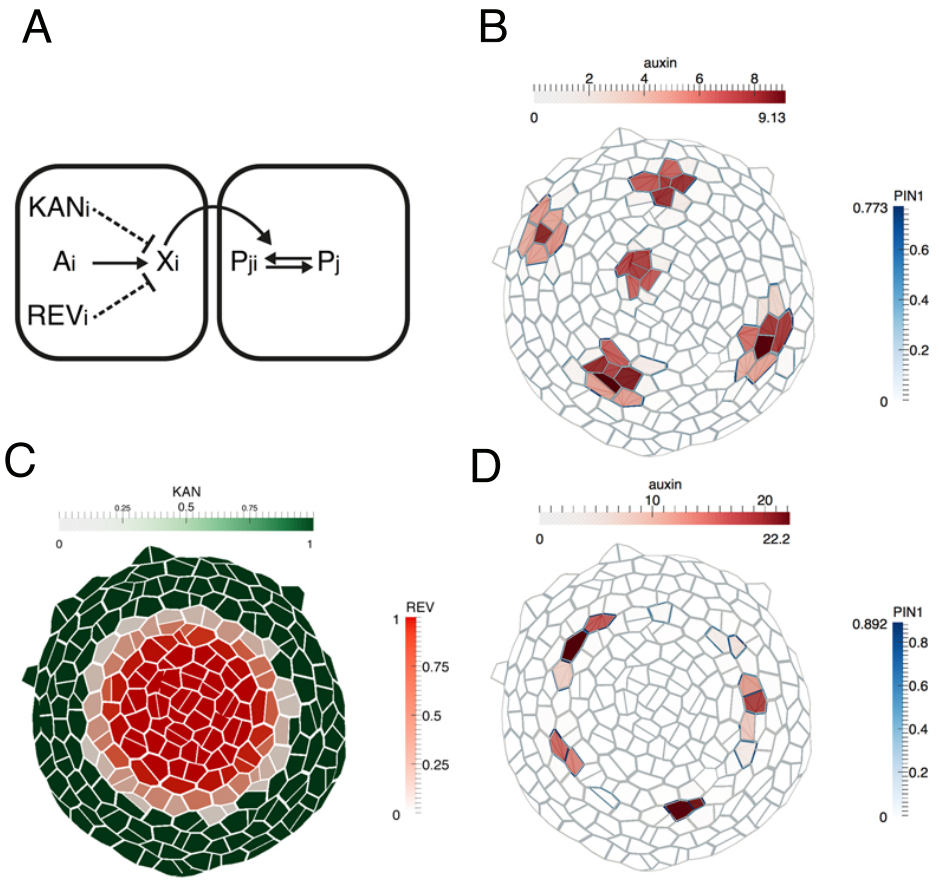

Figure 8.

Computational model illustrating how dorsoventral gene expression boundaries may restrict phyllotactic patterning to the SAM peripheral zone.

(**A**) Illustration of model interactions. Auxin is transported passively and actively via PIN1 between cells. PIN1 is polarized towards cells with high auxin, via a signaling pathway represented by X (previously suggested to be realized by increased stresses in the neighboring cells due to changes in mechanical wall properties (Heisler et al., 2010). (**B**) As shown previously (Heisler et al., 2010; Jonsson et al., 2006; Smith et al., 2006), peaks of auxin are formed spontaneously. (**C**) A pattern of KANADI (green) and REVOLUTA (red) is added to the template with a boundary domain in between in which REV expression is low or absent and KAN1 expression is absent. (**D**) If KANADI and REVOLUTA decrease the signal X in cells where they are expressed (dashed interactions in A), the formation of auxin peaks is restricted to the boundary.

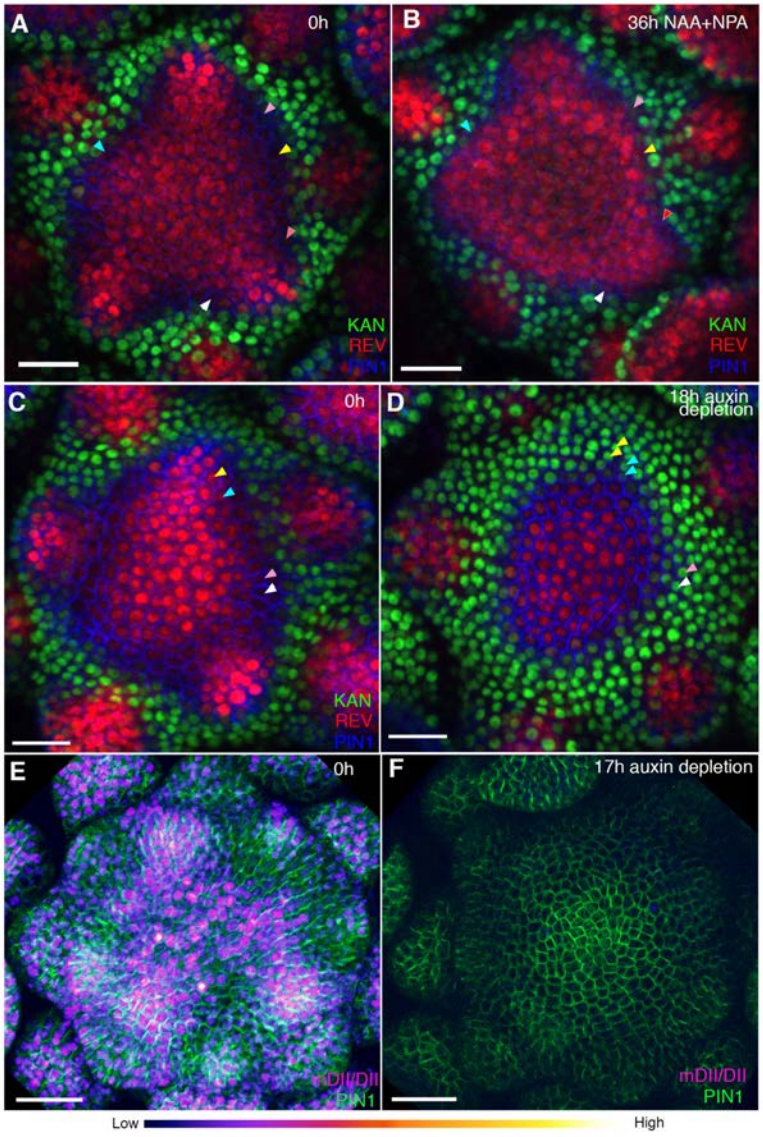

Figure 9.

Effect of auxin addition and depletion on the expression pattern of DV genes.

(A and B) Confocal projections of the IMs showing expression pattern of REV-2×YPet (red), KAN1-2×GFP (green) and PIN1-CFP (blue) before (A) and 36 hours after the combined application of 5mM NAA and 100µM NPA (B). Note REV expression has broadened slightly after the application of NAA and NPA combination (compare regions marked by arrow heads in (A) vs (B) (n=2/3). **(C and D)** Confocal projections of the IMs showing expression pattern of REV-2×YPet (red), KAN1-2×GFP (green) and PIN1-CFP (blue) before (C) and 48 hours after the combined application of 100µM auxinole, 100µM KYN and 100µM Yucasin (auxin depleting drugs). Note KAN-2×GFP expression

952 has expanded centrally at the expense of REV-2×YPet expression (compare the cells
953 marked by arrowheads in (C) with (D), similar colored arrowheads mark the same cells
954 tracked over 48 hours) (n=6/6) **(E and F)** Confocal projections of the IMs indicating the
955 predicted auxin distribution (magenta) based on R2D2 expression along with PIN1-GFP
956 expression (green) before (E) and 17 hours after the combined application of 100μM
957 auxinole, 100μM kyn and 100μM yucasin (auxin depleting drugs) (F). Note lack of
958 detectable auxin based on R2D2 expression in (F) compared to (E) after drug application
959 (n=3/4). Scale bars 20μm (A-D), 30μm (E and F).
960

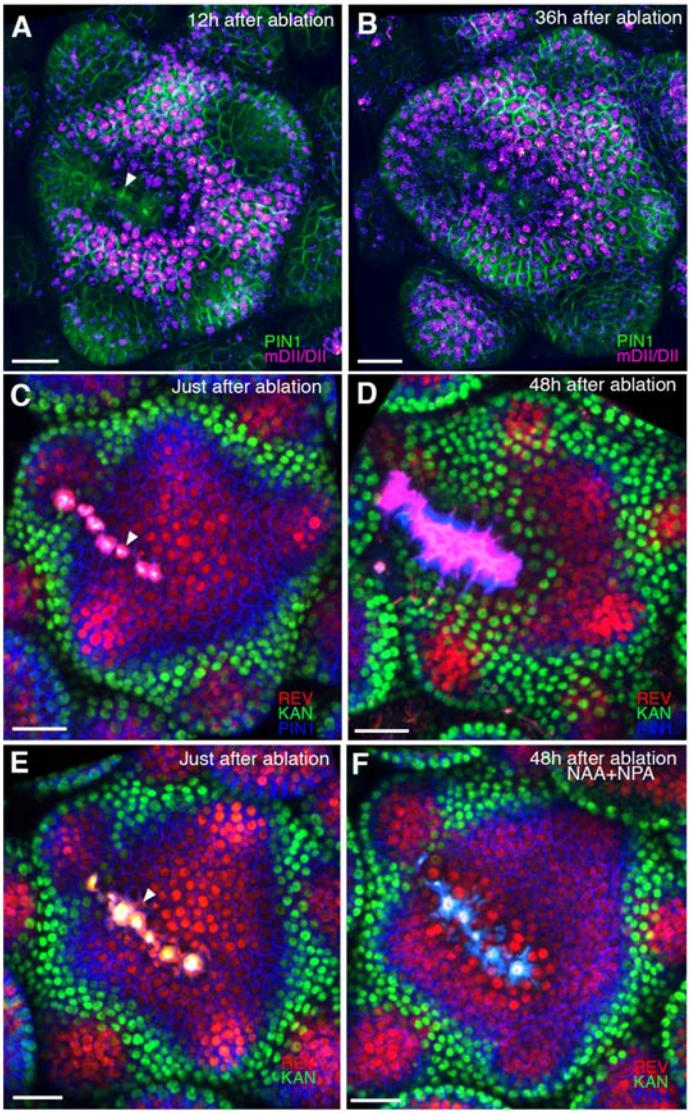

Figure 10.

Wounding induces auxin depletion dependent KANADI1 expression.

(A and B) Confocal projections of IMs showing predicted auxin distribution (magenta) based on R2D2 expression 12hours (A) and 36 hours (B) after wounding. Note low predicted auxin levels in the cells surrounding the ablated cells. **(C and D)** Confocal projections of the IMs showing expression pattern of REV-2×YPet (red), KAN1-2×GFP (green) and PIN1-CFP (blue) immediately after ablation (ablated cells are marked by white arrowheads) (C) and 48 hours after. Note KAN1 expression (green) has completely surrounded the wounded cells 48h after the ablation (D) compared to (C). **(E and F)** Confocal projections of the IMs showing expression pattern of REV-2×YPet (red),

972 KAN1-2×GFP (green) and PIN1-CFP (blue) immediately after ablation (ablated cells are
973 marked by white arrowheads) (E) and 48 hours after ablation and combined NAA and
974 NPA application (F). Note absence of KAN1 expression (green) surrounding the wound
975 when wounding is accompanied by the exogenous addition of auxin and NPA (compare
976 to (D)). Scale bars 30μm (A-F).
977

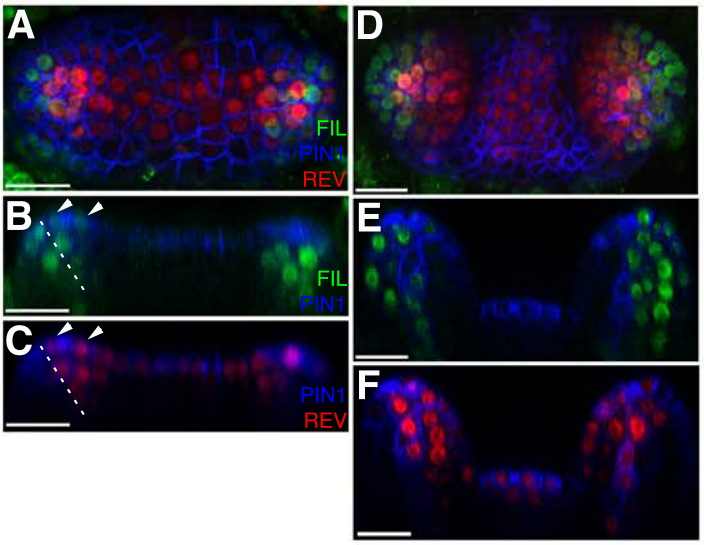

Supplementary Figure S1.

***FILp::dsREDN7* expression is broad during leaf initiation but is later excluded from dorsal tissues**. **(A-F)** Confocal projections and reconstructed sections of seedlings expressing *FILp::dsREDN7* (green), REV-2×VENUS (red) and PIN1-CFP (blue). **(A)** Top view of seedling at 3DAS **(B to C)** Longitudinal section of seedling shown in (A). Dashed line shows dorsoventral axis of first leaf and arrowheads mark dorsal cells expressing both REV-2×VENUS and *FILp::dsREDN7*. **(D)** Seedlings at 3.5 DAS with *FILp::dsREDN7* expression more restricted to the developing ventral side of the leaf. **(E to F)** Longitudinal sections of seedling shown in (D) showing a more complementary pattern of *FILp::dsREDN7* relative to REV-2×VENUS compared to the earlier stage shown in (A) to (C). Scale bars represent 20 µm.

991

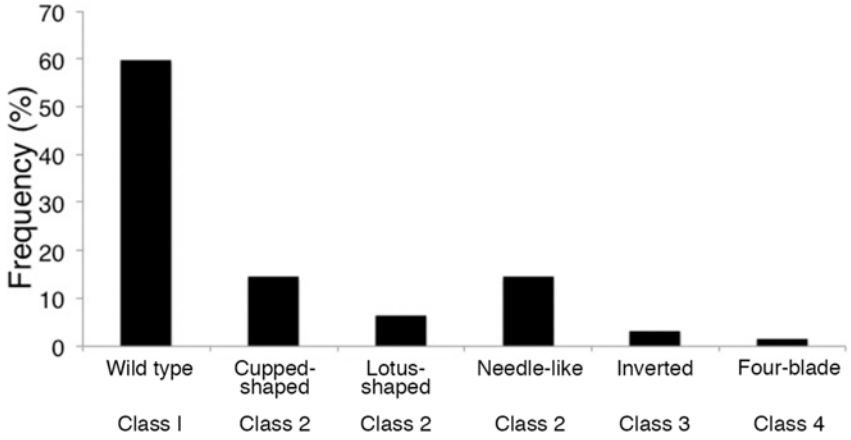

992

993 **Supplementary Figure S2.**

994 Frequency of seedlings exhibiting different leaf morphologies after ectopic induction of
995 KAN1-2×GFP expression in the CLV3 domain (see Figure 6). Class of phenotype
996 corresponds to those indicated in Figure 6. I to O.

997

998

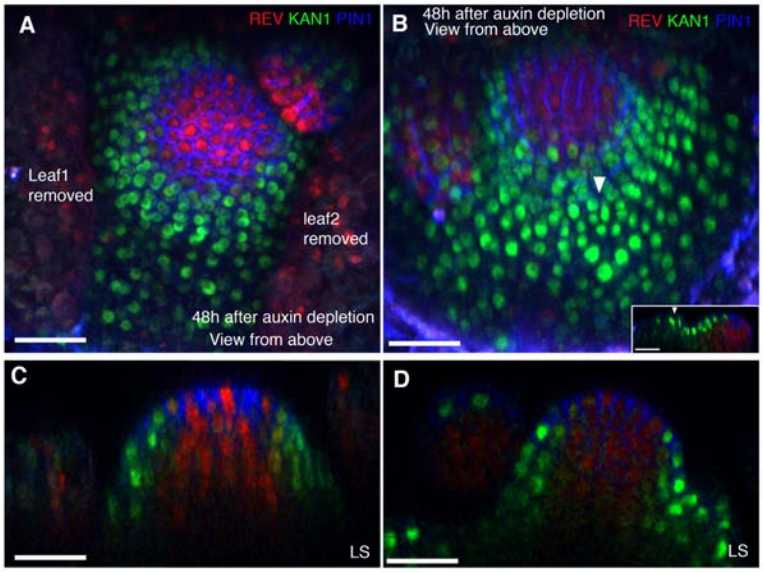

999

1000 **Supplementary Figure S3.**

1001 **Auxin depletion results in altered patterns of dorsoventral gene expression in**
1002 **vegetative meristems.**

1003 **(A and B**) Confocal projections of the VMs showing expression pattern of REV-2×YPet
1004 (red), KAN1-2×GFP (green) and PIN1-CFP (blue) 48 hours after the combined
1005 application of 100µM auxinole, 100µM KYN and 100µM Yucasin (auxin depleting
1006 drugs). Arrowhead in (B) marks an arrested leaf primordium expressing KAN
1007 throughout. Inset in (B) shows a longitudinal optical section of the leaf primordium
1008 ectopically expressing KAN1-2×GFP. **(C and D)** Longitudinal optical sections of the
1009 VMs in (A) and (B) respectively. Note that the meristems grow as pins with no new
1010 organs initiating. Scale bars 30µm (A-D, inset in B).

1011

1012

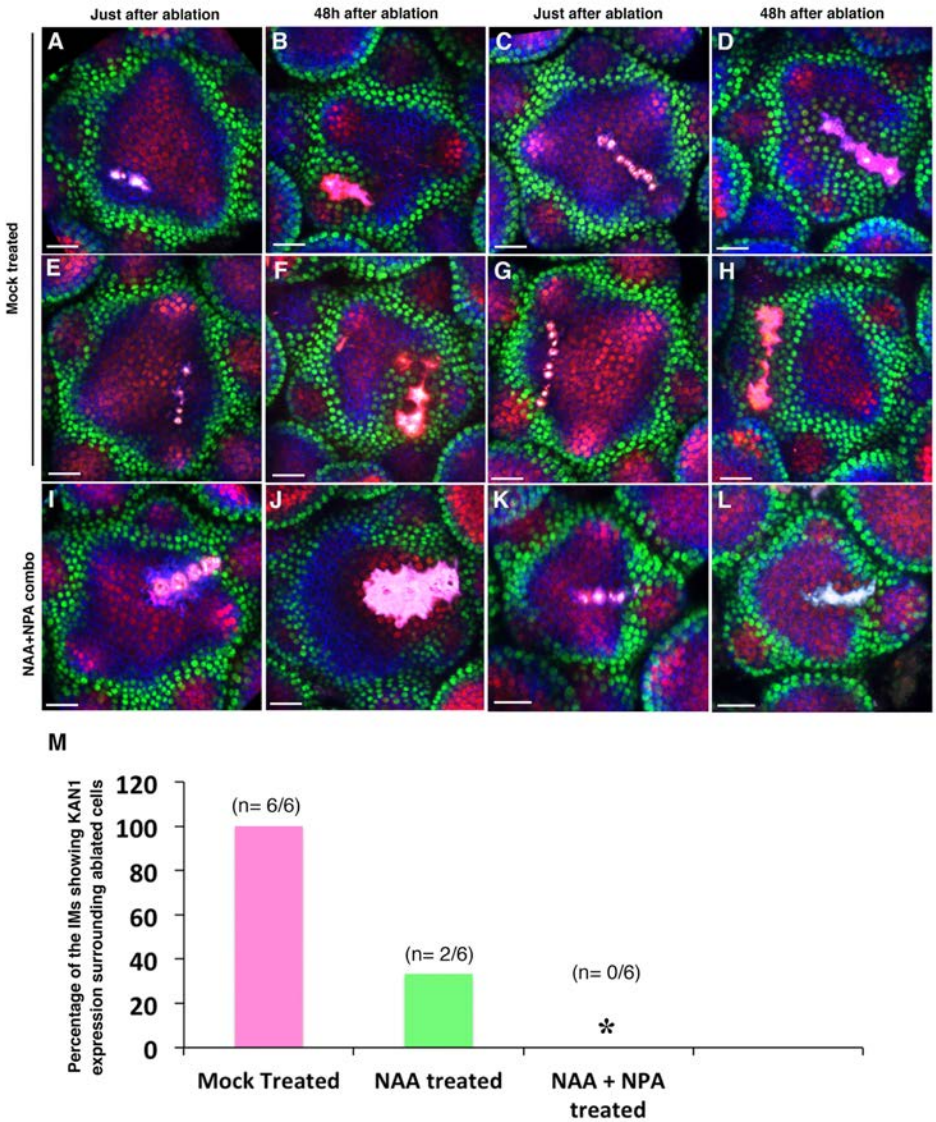

1013

1014 **Supplementary Figure S4**.

1015 **Wounding induces ectopic KAN expression in inflorescence meristems.**

1016 (**A-H**) Confocal projections of the inflorescence meristems showing expression pattern
1017 of KAN1-2×GFP (green) and PIN1-CFP (blue) immediately after ablation (A, C, E, and
1018 G) and corresponding meristems 48 hours after ablation (B, D, F and H). Note ectopic
1019 KAN1 expression on both the sides of the ablated cells 48 hours after wounding. (**I-L**)
1020 Confocal projections of inflorescence meristems showing expression pattern of KAN1-
1021 2×GFP (green) and PIN1-CFP (blue) immediately after (I and K) and 48 hours after
1022 ablation and treatment with NAA and NPA (J and L). Note lack of ectopic KAN1

1023 expression compared to comparable untreated meristems (B, D, F and H). (**M**)
1024 Quantification of wounding induced ectopic KAN1 expression upon mock treatment
1025 (n=6/6)), NAA application (n=2/6)) and NAA + NPA combination (n= 0/6) application
1026 on the Arabidopsis IMs expressing REV-2×YPet, KAN1-2×GFP and PIN1-CFP. Scale
1027 bars 20μm (A to L).
1028

1029

1030

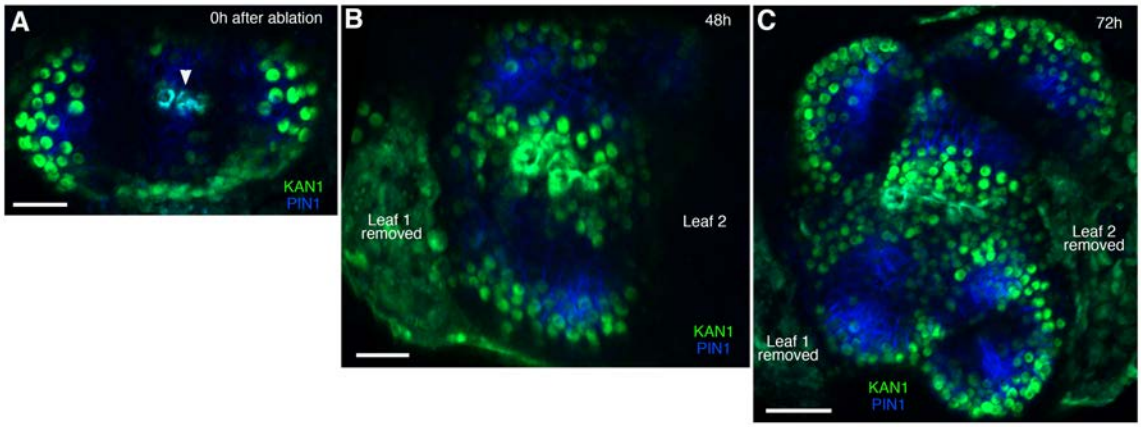

1031

1032

1033 **Supplementary Figure S5**.

1034 **Wounding induced ectopic KAN expression and reorganization of the vegetative**
1035 **meristem.**

1036 (**A-C**) Confocal projections of the vegetative meristems showing expression pattern of
1037 KAN1-2×YPet (green) and PIN1-GFP (blue) immediately after ablation (A), 48 hours
1038 after ablation (B) and 72hours after ablation (C). Ablated cells are marked by arrowhead
1039 in (A). 72 hours after wounding the vegetative meristem appears split into at least two
1040 distinct meristems with new leaves oriented normally with respect to each meristem (C).
1041 Scale bars 20μm (A and B); 30μm (C).

1042

1043

Table S1.

Primers for cloning and Q-PCR

Gene	Primer name	Sequence
KAN1 (At5g16560)	KAN1g F	ACGCGTTGTTTGGATGTATGACATTAAGTAAGCTAT
KAN1 (At5g16560)	KAN1g R	GGATCCGCTTTCTCGTGCCAATCTGGTCTGCCTAA
KAN1 (At5g16560)	K1cDNA F	AGATCTAACAATGTCTATGGAAGGTGTTTTCCTAGAGAAAAC
KAN1 (At5g16560)	K1 cDNA R	GGATCCGCTTTCTCGTGCCAATCTGGTCTGCCTAA
CLV3 (At2g27250)	CLV3p F	GGAATTCCGGATTATCCATAATAAAAAC
CLV3 (At2g27250)	CLV3p R	CTGCAGGTTTTAGAGAGAAAGTGACTGAGTGA
CLV3 (At2g27250)	CLV3utr F	AAACCTGCAGGGATCCGCGGC
CLV3 (At2g27250)	CLV3p R	ATAGAATATCACTAGTTAATTATCATTGGTTTAAAGTTATAG
WOX1 (At3g18010)	WOX1p F	ggtaccTCAAAACCGGTTTTTATACGACAAGAC-
WOX1 (At3g18010)	WOX1p R	ggatccTTTGGTGTGTACTTAATTTATATGTATG
WOX1 (At3g18010)	WOX1g F	gcggcagcaagatctATGTGGACGATGGGTTACAACGAAG
WOX1 (At3g18010)	WOX1g R	atagaatatcactagtACGTCACTGATGATATACTACG
PRS (At2g28610)	PRSg F	agatctGCGTACGTGTGTACGTGAATGAAAT
PRS (At2g28610)	PRSg R	ggatccAGTTTGGTACTGTCTTGTTTGGAGT
PRS (At2g28610)	PRS FP (Q-PCR)	CAACTCCAAACAAGACAGTACCA
PRS (At2g28610)	PRS RP (Q-PCR)	ACATGAATGAAACACCTGCAGA
WOX1 (At3g18010)	WOX1 FP (Q-PCR)	GCCTCCTTCGTTGTAACCCA
WOX1 (At3g18010)	WOX1 RP (Q-PCR)	GCTGTCTCTCTCCCTTCTCC
IAA20 (At2g46990)	IAA20 FP (Q-PCR)	ATGTGCAATGAGAAGAGTCACG
IAA20 (At2g46990)	IAA20 RP (Q-PCR)	TCACAGTAGACAAGAACATCTCC
ACT2 (At3g18780)	ACT2 FP (Q-PCR)	CCTGTTCTTCTTACCGAGGC
ACT2 (At3g18780)	ACT2 RP (Q-PCR)	AATTTCCCGCTCTGCTGTTG

1044

1045

1046

Table S2.
Frequencies of phenotypes amongst transgenic plant lines

Transgenic plants	N° of T2 lines	T2 line phenotypes
ATML1>>REVr-2×VENUS	31	15 arrest or delay of organogenesis 8 partially or completely dorsalized leaves only 8 no phenotype
UBQ10>>STTM 165/166	26	6 arrested organogenesis 20 partially or completely dorsalized leaves
ATML1>>PHVr	50	4 arrest or delay of organogenesis 31 partially or completely dorsalized leaves 15 no phenotype
ATML1>>KAN1-GFP	17	11 meristem arrest 6 partially or fully radialized organs only
CLV3>>KAN1-2×GFP	32	10 mild change in organ position 10 meristem arrest only 12 leaf morphology change and meristem arrest

For *ATML1>> REVr-2×VENUS* (n=20, number of imaged specimens) and *UBQ10>>STTM 165/166* (n=12) transgenic plants, we used T3 generation plants for imaging that exhibited the reported phenotypes at a frequencies ranging from 70 to 90%. For *ATML1>>KAN1GFP* transgenic plants, we imaged a particular T2 line that exhibited meristem arrest after induction at a frequency of approximately 98% (n=10). For *CLV3>>K2G* transgenic lines, among 12 different T2 lines that showed leaf morphology changes and meristem arrest, we used a particular line that produced more than two leaves after meristem arrest at a frequency of 96.8% (n=65). For *ATML1>>PHVr* transgenic lines, we imaged a line that exhibited arrested organogenesis at a frequency of 33% (n=12). An absence of phenotype was generally associated with low levels of induced transgene expression.

1047

1048

Table S3
List of parameter values used in simulations. We have used the values from Heisler and Jönsson (2006), which are based on experimental estimates where applicable.

Symbol	Value	Description
c_A	0.001	Auxin production
d_A	0.001	Auxin degradation
T	1.3	Active transport of auxin (PIN1-dependent)
D	0.002	Passive transport of auxin
c_P	0.001	PIN1 production
d_P	0.001	PIN1 degradation
V_X	10.0	Maximal production rate of polarising signal X
K_{XA}	10.0	Hill constant for auxin activating X
n_{XA}	1	Hill coefficient for auxin activating X
K_{XR}, K_{XK}	0.1	Hill constants for REV/KAN repressing X
n_{XR}, n_{XR}	2	Hill coefficients for REV/KAN repressing X
d_X	1.0	Degradation of polarising signal X
k_p	0.9	Relation of symmetric vs polarized PIN1
f_p	0.3	Ratio between PIN1 endo/exocytosis

1075 **Table S4 Statistical details for RT PCR experiment**
1076

	PRS	WOX1	IAA20
Rep1 FC	1.678900384	1.478510137	2.679542279
Rep2 FC	3.216883524	1.991086008	3.602300305
Rep3 FC	1.735102699	3.763611201	2.629479589
Rep4 FC	3.016883524	1.665693641	2.923774058
Rep5 FC	1.335102699	3.099714601	2.479542279
Mean	2.196574566	2.399723118	2.862927702
SD	0.856885899	0.988002492	0.44313845
p-value	0.0142	0.0132	0.0001
Median	1.735102699	1.991086008	2.679542279
SEM	0.383211024	0.441848147	0.198177539
N	5	5	5
95% confidence intervals			
Upper limit	2.947668173	3.265745486	3.251355679
Lower limit	1.445480959	1.53370075	2.474499725

1077
1078

Movie S1

Movie shows confocal 3D projection of a single vegetative seedling corresponding to that shown in Fig. 6, G and H. Several leaf-like organs have formed on the boundary of ectopic KAN1 expression driven by the CLV3 promoter (green). These organs express REV (red) in restricted patterns corresponding to the three classes described in Fig. 6 (labeled Class 2, 3 and 4). Note developing leaf margins, marked by high PIN1 expression (blue) correlate with REV expression boundaries in the epidermis.

Computational model files (separate file as one zipped archive)

Archive containing files used for the computational model. Files will be extracted to the directory modelFiles, and further information is found in the file README.txt in this directory.

1096

1097